Paleoceanography and Paleoclimatology

RESEARCH ARTICLE
10.1029/2019PA003605

Key Points:
- The sea-ice cover in the northeastern Labrador Sea appears to only have varied on millennial timescales between H5 and H4
- Heinrich-like calving events are only evident related to H4 and H3, not H6 and H5
- Enhanced influence of Atlantic water during Greenland interstadials 14, 12 and 8

Supporting Information:
- Supporting Information S1

Correspondence to:
L. Griem,
lisa.griem@uib.no

Citation:
Griem, L., Voelker, A. H. L., Berben, S. M. P., Dokken, T. M., & Jansen, E. (2019). Insolation and glacial meltwater influence on sea-ice and circulation variability in the northeastern Labrador Sea during the last Glacial period. *Paleoceanography and Paleoclimatology*, *34*, 1689–1709. https://doi.org/10.1029/2019PA003605

Received 12 MAR 2019
Accepted 19 SEP 2019
Accepted article online 19 OCT 2019
Published online 1 NOV 2019

Insolation and Glacial Meltwater Influence on Sea-Ice and Circulation Variability in the Northeastern Labrador Sea During the Last Glacial Period

Lisa Griem[1], Antje H. L. Voelker[2,3], Sarah M. P. Berben[1], Trond M. Dokken[4], and Eystein Jansen[1,4]

[1]Department of Earth Science, University of Bergen, Bjerknes Center for Climate Research, Bergen, Norway, [2]Divisão de Geologia e Georecursos Marinhos, Instituto Português do Mar e da Atmosfera (IPMA), Lisbon, Portugal, [3]Centre of Marine Sciences (CCMAR), Universidade do Algarve, Faro, Portugal, [4]NORCE Climate, NORCE Norwegian Research Centre AS, Bjerknes Center for Climate Research, Bergen, Norway

Abstract The variable amounts of ice rafted debris (IRD) and foraminifers in North Atlantic sediments are related to the abrupt, millennial-scale alteration from Greenland stadials to interstadials during the last glacial period and indicate past ice sheet instabilities, changes in sea-ice cover and productivity. In the Norwegian Sea, Greenland stadials were likely characterized by an extensive, near-perennial sea-ice cover whereas Greenland interstadials were seasonally ice-free. The variability in other areas, such as the Labrador Sea, remains, however, obscure. We therefore investigated deep-sea sediment core GS16-204-22CC retrieved south of Greenland. Using a multiproxy approach, we distinguish two sediment regimes and hence different environmental conditions between ca. 65 and 25 ka b2k. Regime 1 (~65-49 ka b2k) is characterized by the dominance of planktic foraminifers in the sediments. During late MIS4 and early MIS3, the site was covered by near-perennial sea-ice with occasional periods of iceberg discharge. During the younger part of regime 1 the northeastern Labrador Sea was seasonally ice-free with hardly any icebergs melting near the site and long-term environmental conditions were less variable. Regime 2 (~49-25 ka b2k) is characterized by pronounced stadial-interstadial variability of foraminifer and IRD fluxes, suggesting an extensive sea-ice cover during most Greenland stadials and seasonally ice-free conditions during most Greenland interstadials. During MIS2 environmental conditions were very similar to those of the younger part of regime 1. While all Heinrich (H) related Greenland stadials are marked by depleted oxygen isotope values at our core site, only H4 and H3 are associated with pronounced IRD peaks.

Plain Language Summary North Atlantic sediments contain variable amounts of sand-sized mineral grains and microorganism shells. Mineral grains indicate iceberg transport from continental ice sheets, like the Greenland ice sheet (more icebergs/melting sea-ice, more grains). If the sea-ice cover is too thick, no light can penetrate and fewer microorganisms live in the water beneath the ice. Using these indicators, we investigated ocean sediments from south of Greenland covering the time period between ca. 65 and 25 thousand years ago. This time period was characterized by several abrupt changes between cold and warm climates on millennial timescales. We find that the ocean south of Greenland was sea-ice covered for most of the year with occasional time periods of iceberg discharge between 65 to 56 thousand years ago. From 56 to 49 thousand years ago the ice-free season was extended and hardly any icebergs melted near the site. From 49 thousand years ago our study area was covered by sea-ice year-round during cold time intervals whereas warm time intervals were only seasonally sea-ice covered. Continental ice sheets were growing during this time interval and we observed two major calving events related to two of the four very cold climate intervals recorded in the analyzed sediment.

1. Introduction

Freshwater influx sourced from ice-sheet instabilities and melting sea-ice has an impact on surface and deep ocean circulation and hence, on global climate. A key area to investigate such dynamics is the Labrador Sea, as it is both a region susceptible to climate change and the location for several key circulation processes. The Labrador Sea is a locus of deep-water formation and plays a role as conduit for deep sea flows and hosts

interactions between warm and cold surface currents. The region comprises a mix of water masses of distinct origin: warmer and more saline Atlantic water, and cooler and fresher Arctic waters (Dickson et al., 2002).

During the last glacial period the North Atlantic region experienced changes in sea surface hydrology as a response to abrupt climate changes (Cortijo et al., 1997), and consequently expanded sea-ice distribution and drifting ice bergs (Bond, 1997). Abrupt climate changes as recorded in Greenland ice cores (Dansgaard-Oeschger (DO) events, Dansgaard et al., 1993) might have been driven by changes in the Nordic Seas sea-ice extent (Dokken et al., 2013; Hoff et al., 2016; Sadatzki et al., 2019). Reduced sea-ice formation during Greenland interstadials allowed for a northward heat transport and subsequent loss of oceanic heat to the atmosphere, whereas during Greenland stadials, a more extended sea-ice cover resulted in a reduced heat exchange. Thus, it is often assumed by model studies that sea-ice has continuously covered the Labrador Sea and extended as far south as 50°N during both Greenland stadial and interstadial conditions (Vettoretti & Peltier, 2016). Along the ice edge, melting icebergs, originating from the ice stream collapses of the Laurentide and Eurasian ice sheets, delivered pronounced amounts of ice rafted debris (IRD) to an area of the North Atlantic known as the Ruddiman belt (55 to 40°N; Bond et al., 1993; Hemming, 2004; Ruddiman, 1977). Prominent layers of IRD coincide with the coldest Greenland stadials every 7 to 15 ka (Bond et al., 1992; Heinrich, 1988; Rashid et al., 2003b). These IRD events are characterized by collapsing ice sheets and possible reduction in overturning circulation, and are referred to as Heinrich (H) events. Over the last glacial cycle six H-layers (H1 to H6) were identified (e.g. Böhm et al., 2015; Rahmstorf, 2002). The main contributor to the IRD-rich H-layers was the Laurentide ice sheet, except for H3 and H6 where the IRD content potentially had a Eurasian source (Hemming, 2004 and references therein). However, the Greenland ice sheet´s contribution to H-layers and IRD influx in general during MIS3 are still obscure, while proxy evidence from the Labrador Sea is non-existent.

Proxy data from the Labrador Sea is required to evaluate potential future climate responses, including the sensitivity of the Greenland ice sheet to rising Arctic temperatures and the impact of a higher freshwater influx on deep-water formation. Evidence from this region can help improve reconstructions of oceanic front boundaries, sea-ice cover fluctuations and ice sheet instabilities, as well as the similarities and differences between the individual Greenland stadials and interstadials. This knowledge is important for model simulations in order to constrain the boundary conditions of abrupt climate changes and lead to a better understanding of today´s abrupt warming and its consequences. To date, the lack of proxy evidence from the Labrador Sea leads to model simulations of climate parameters like sea-ice extent or sea surface temperatures that cannot be validated (e.g. Bagniewski et al., 2017; Drijfhout et al., 2013; Kleppin et al., 2015).

In addition to the unknown variability of the sea-ice cover and surface hydrography in the Labrador Sea, it also remains uncertain whether the Greenland ice sheet reached the continental shelf edge between MIS6 and MIS2 (Funder et al., 2004; Vasskog et al., 2015). It was suggested that the Greenland ice sheet constantly grew throughout MIS3 whereby rapid responses are limited to the ice margins and were caused by rapid forcings (Alley et al., 2010; Ganopolski et al., 2010). Hereby, the sensitivity of the ice margins to climate changes varies geographically, depending on shelf bathymetry and drainage, sea surface temperatures in the vicinity of the ice sheet, sea-level, sea-ice conditions, etc. (Funder et al., 2011). Marine-geological investigations by Funder et al. (2004) suggested that the Greenland ice sheet reached the northern and southeastern shelves at ca. 31 ka b2k and the southwestern to northwestern shelf ca. 10 ky later. To our knowledge, no proxy evidence supporting a Greenland ice sheet collapse similar to those of the Laurentide or Eurasian ice sheets exists. All MIS3 calving events recorded along the East Greenland margin show a similar amplitude and seem to follow a millennial timescale whereby an enhanced IRD input was observed for both Greenland interstadials and stadials (e.g. Elliot et al., 1998; Elliot et al., 2001; Voelker et al., 1998). However, the IRD input could have been hampered by too cold sea-surface temperatures or sea-ice which, according to Dokken et al. (2013), might have covered the Denmark Strait during both Greenland interstadials and stadials. Contrarily, the Nordic Seas were seasonally ice-free during Greenland interstadials providing a potential moisture source for the Greenland ice sheet to grow during MIS3 (e.g. Dokken et al., 2013; Li et al., 2010).

Since proxy evidence about changes in calving rates, surface hydrography and sea-ice cover are currently missing from the Labrador Sea for MIS3, no conclusions about the effect of abrupt climate changes on deep-water convection or the size of the Greenland ice sheet can be drawn. Most studies from the Labrador Sea focus on either long-term low-resolution records (e.g. Evans et al., 2007; Hillaire-Marcel et al., 1994; Hillaire-Marcel et al., 2011; Hiscott et al., 2001; Hunter et al., 2007; Müller-Michaelis &

Uenzelmann-Neben, 2014) or high-resolution reconstructions restricted to the Eemian or the period between MIS2 and the Holocene (e.g. de Vernal & Hillaire-Marcel, 2000; Galaasen et al., 2014; Irvalı et al., 2016; Moffa-Sánchez et al., 2014). The main reason for this time gap is that Greenland shelf sediments were eroded to a large extent during the last glacial maximum (Funder et al., 2004; Vasskog et al., 2015). MIS3 proxy data from the northern Labrador Sea are highly relevant in order to connect the millennial-scale changes in the Nordic Seas with the events recorded in the Ruddiman belt and fill in the knowledge gaps related to abrupt climate changes in this region.

In this study, we investigate a deep-sea sediment core from the Eirik drift, northeastern Labrador Sea, for a time period between the end of MIS4 (ca. 65 ka b2k) and the beginning of MIS2 (ca. 25 ka b2k). Using a combination of high-resolution stable isotope data, IRD and foraminifer fluxes and low-resolution planktic assemblage counts we aim to (1) close the time gap between MIS5 and MIS2 as well as the geographical gap of proxy evidence between 60 and 55°N in the Northwestern Atlantic, (2) draw conclusions about the sensitivity of the Labrador Sea in terms of sea-ice extent, surface hydrography and iceberg discharge during MIS3, and (3) connect the proxy records along the east-to-south Greenland margin by comparing our data to marine sediment cores PS2644-5 (Voelker et al., 1998) and SU90-24 (Elliot et al., 1998).

2. Oceanographic Setting of the Study Site

Sediment core GS16-204-22CC-A (58° 02.83 N, 47° 02.36 W, water depth 3160 m, Figure 1; hereafter 22CC) was retrieved at the Eirik drift by R/V *G.O. Sars* (ice2ice, 2016). The Eirik drift is an elongated, mounded ridge system in the northeastern Labrador Sea where sediments from the Denmark Strait and the Greenland margin are deposited by the Deep Western Boundary Current. The Deep Western Boundary Current follows the topography of the Greenland margin towards the toe of the Eirik drift crest whereafter it turns towards the western Labrador Sea. In this process the Deep Western Boundary Current slows down at the Eirik drift, whereby its velocity and pathway depend on climatic conditions (Hunter et al., 2007; McCave & Tucholke, 1986). During glacial periods the sedimentation rates were, in general, higher on the Greenland slope (<2500 m water depth) compared to the Greenland rise (>3000 m water depth). Sedimentation rates for the Greenland rise are estimated at ~7-10 cm/ky during glacial intervals and >30 cm/ky during the Holocene (Hillaire-Marcel et al., 1994; Stoner et al., 1998). However, this might have changed on shorter timescales (Hillaire-Marcel et al., 1994). The combination of this location´s climate sensitivity and high sediment accumulation rates make the Eirik drift ideal for high-resolution paleoclimate studies on multi-decadal timescales.

The study location is further characterized by an interplay of several surface currents (Figure 1). First, the East Greenland Current (EGC) exports freshwater and sea-ice from the Arctic Ocean, via the Denmark Strait, into the North Atlantic (Hopkins, 1991). The cold EGC protects the coastal glaciers of Greenland from the warm water masses of the Irminger Current. The latter turns south of Iceland, and flows subsequently southwards parallel to the EGC. Reaching the southern tip of Greenland, the water masses of both surface currents mix and the surface watermass becomes warmer and saltier with temperatures between 3 and 8°C in present conditions. The surface circulation continues counter-clockwise around Greenland as the West Greenland Current although one-third is retroflected southwards into the subpolar gyre (e.g. Daniault et al., 2016; Garcia-Ibanez et al., 2018; Holliday et al., 2007). The subpolar gyre redistributes freshwater from the Hudson Strait via the Labrador Current and the Arctic via the EGC. In turn, it advects warmer, saline water from the Atlantic into the Labrador Sea and the Nordic Seas via the Irminger Current and the North Atlantic Current, respectively (e.g. Born & Mignot, 2012; Hátún et al., 2005; Huck, 2010).

The subpolar gyre may have been important in driving DO-events. Its strength and lateral expansion are dependent on atmospheric winds, surface heat exchange and freshwater input whereby all those mechanisms are influenced by sea-ice (Li & Born, 2019). Following Li and Born (2019), an expanded sea-ice cover at our core location would introduce a freshwater perturbation that would weaken deep-water convection, the subpolare gyre and thus the northward transport of heat and salt into the Labrador Sea and Nordic Seas. Such a weakening was found under present conditions (Rhein et al., 2011; Thornalley et al., 2018) as well as during past warm periods (Born et al., 2011). While the glacial subpolar gyre has played a crucial role for freshwater distribution, it was also important for the dispersal of icebergs. Under favorable sea surface

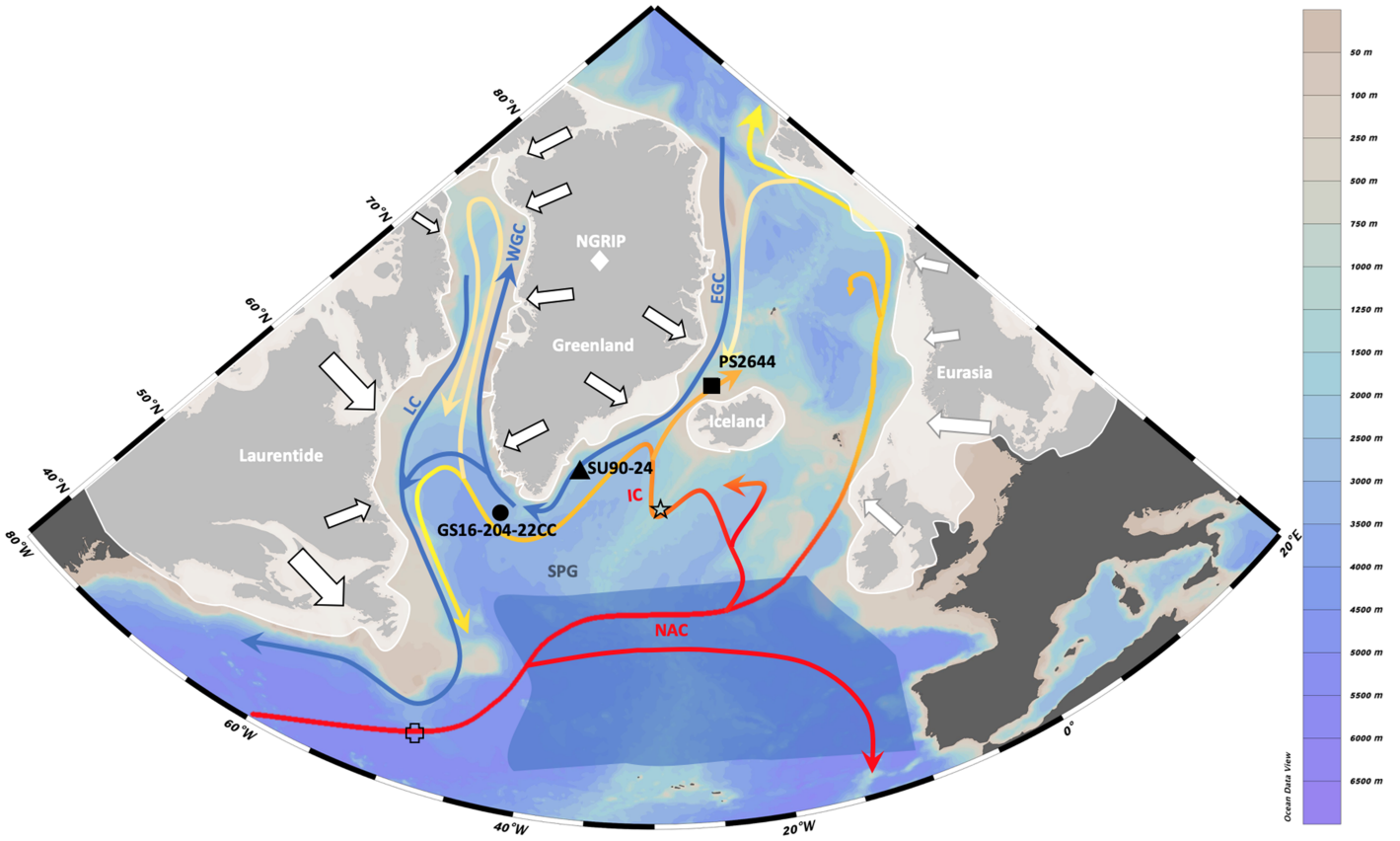

Figure 1. Map of study area from Ocean data view (Schlitzer, 2015) including surface currents (Straneo et al., 2012 and references therein), location of the Ruddiman belt during MIS3 (dark blue shading, Ruddiman, 1977), the late MIS3 ice sheet extent for Greenland, Laurentide, Eurasia and Iceland (modified after Patton et al., 2016 and references therein) and location of sediment cores GS16-204-22CC (this study, circle), PS2644-5 (Voelker et al., 1998, square), SU90-24 (Elliot et al., 1998, triangle), CH69-K09 (Labeyrie et al., 1999, cross), SO82-05 (van Kreveld et al., 2000, star) and ice core NGRIP (white diamond). LC: Labrador Current, WGC: West Greenland Current, EGC: East Greenland Current, IC: Irminger Current, NAC: North Atlantic Current. Arrows indicate flow direction. White arrows indicate major iceberg sources during the last glacial period (Andrews, 2000).

temperature and wind conditions in the North Atlantic, even icebergs from the European ice sheet were transported towards the Labrador Sea (Death et al., 2006).

3. Material and Methods

3.1. Core Description and Sample Preparation

The 1964 cm long calypso core 22CC covers a time interval that spans the early Holocene to approximately the late MIS6. The lower age estimate is based on a distinct red layer at 1670 cm that has previously been observed in other cores from the Labrador Sea and Orphan Knoll and is suggested to have been deposited during early MIS5e (Channell et al., 2012; Nicholl et al., 2012). The core was sampled every 2 cm between 200 and 530 cm with a sample width of 0.5 cm. Bulk sample weights were taken prior to and after freeze-drying. Subsequently, the dried sediment was wet sieved over a 63 μm sieve, whereby the fine fraction was captured. The coarse fraction was dry sieved into size fractions 63-106 μm, 106-150 μm, 150-500 μm, 500-1000 μm and > 1mm, respectively. The weight of drop stones >5 mm was documented separately.

3.2. Radiocarbon Ages

Radiocarbon dating was performed at Beta Analytic Inc., Miami, US and at W. M. Keck Carbon Cycle Accelerator Mass Spectrometry Facility of University of California, Irvine, US (KCCAMS/UCI), respectively. Altogether eleven samples of surface-dwelling polar species *N. pachyderma* (formerly referred to as *N. pachyderma* sinistral, 150-500 μm) were dated. Information regarding the dated material is summarized in Table 1. The AMS ^{14}C ages were calibrated using the Marine13 calibration curve (Reimer et al., 2013) whereby no

Table 1
AMS ^{14}C Ages (Adjusted to b2k by Adding 50 Years) According to the Depths in Sediment Core GS16-204-22CC-A From the Eirik Drift Including, AMS ^{14}C Ages, Calendar Ages, Age Model Ages and the Offset Between the Calendar Age and Our Age Model. In the Right Column the Name of the Laboratory as Well as the Sample Weights are Given

Mean depth (cm)	AMS ^{14}C age (ka b2k)	Calendar age[a] (error 2σ) (ka b2k)	Age model age (ka b2k)	Offset age model from cal. age (ka b2k)	Laboratory (sample weight)
150.5	13.10 ± 0.05	15.09 (14.82 to 15.28)	15.09	0	BETA (5.3 g)
200.25	23.60 ± 0.10	27.49 (27.28 to 27.70)	25.43	-2.06	Keck (7.7 g)
230.25	28.56 ± 0.11	31.89 (31.52 to 32.45)	31.89	0	Keck (9.6 g)
300.25	30.42 ± 0.27	34.10 (33.68 to 34.60)	39.80	5.70	Keck (6.0 g)
370.25	35.48 ± 0.28	39.61 (38.90 to 40.27)	46.04	6.44	Keck (4.9 g)
410.25	48.75 ± 2.50	Outside cal. range	49.62	-	Keck (6.5 g)
450.25	46.98 ± 0.89	Outside cal. range	53.22	-	Keck (9.2 g)
500.5	35.64 ± 0.30	Too young	58.21	-	BETA (6.3 g)
600.25	52.25 ± 1.70	Outside cal. range	Outside investigation period	-	Keck (7.3 g)
640.25	57.55 ± 3.20	Outside cal. range	Outside investigation period	-	Keck (9.5 g)
1000.5	44.60 ± 0.90	Too young	Outside investigation period	-	BETA (5.2 g)

[a]Marine13 (Reimer et al., 2013).

local reservoir corrections were applied. For this study, the calibrated BP (before present=1950 AD) ages were converted to b2k (before 2000 AD) ages by adding 50 years.

3.3. Stable Isotope Measurements

Stable isotope analysis was carried out in the laboratory facilities of FARLAB at the Department of Earth Sciences, University of Bergen, Norway using a ThermoFinnigan MAT253 gas source isotope ratio mass spectrometer. The long-term analytical precision of the instrument is ±0.04‰ and ±0.02‰ for $\delta^{18}O$ and $\delta^{13}C$, respectively, based on repeated analysis of in-house standard CM 12 and IAEA standard NBS 18. The results are reported relative to the VPDB scale.

Eight to ten encrusted planktic *N. pachyderma* specimens (50-80 μg) ranging in size from 212 to 250 μm were selected for stable isotope analysis. The foraminifer tests were rinsed with methanol and cleaned in an ultrasonic bath for ten seconds. Isotope measurements were performed on samples between 200 and 600 cm at intervals of 2 cm.

Although the habitat depth of *N. pachyderma* is quite variable and driven by sea-ice and the concentration of chlorophyll (Greco et al., 2019), it is usually concentrated around an isopycnal layer with water densities between 27.7 and 27.8 (σ_τ, Kozdon et al., 2009) at water depths between 70 and 130 m below the fresh EGC. However, depleted planktic $\delta^{18}O$ values might indicate a conservative estimate of meltwater input (Simstich et al., 2003). The planktic $\delta^{18}O$ signal is a function of salinity and temperature and therefore, depleted planktic $\delta^{18}O$ values can also indicate an increased inflow of warm Atlantic water and thus represent a shift between oceanic fronts (Johannessen et al., 1994).

3.4. IRD and Foraminifer Abundances

IRD and foraminifers were counted between 200 and 530.5 cm at 2 cm resolution (total of 166 samples) in the size fractions 150-500 μm, 500-1000 μm and >1mm. In the 150-500 μm fraction about 400 to 1500 grains were counted for both total IRD and foraminifers depending on the number of splits (0-4). The results are reported in number of grains >150 μm g^{-1} dry sediment (combining the three counted size fractions, supporting information and Figure 3) and as fluxes (Figures 4 and 5). Here, IRD consists of the number of lithic grains although volcanic grains were counted separately in order to identify tephra layers. Drop stones (>5 mm) were found throughout the record weighing between 0.2 g and 8.1 g with a size up to 2.5 cm (~38.5 ka b2k). Due to their high impact on the dry bulk sediment weight and their diameter larger than the sample width (0.5 cm), they were not considered for the calculation of IRD and foraminifer abundances. Despite the background noise of IRD throughout the core resulting from the proximity of the Greenland ice sheet, high IRD concentrations occur due to icebergs from calving ice sheets and along the sea-ice edge (Dowdeswell et al., 1998; Ramseier et al., 2001). The lowest IRD concentrations occur during periods of

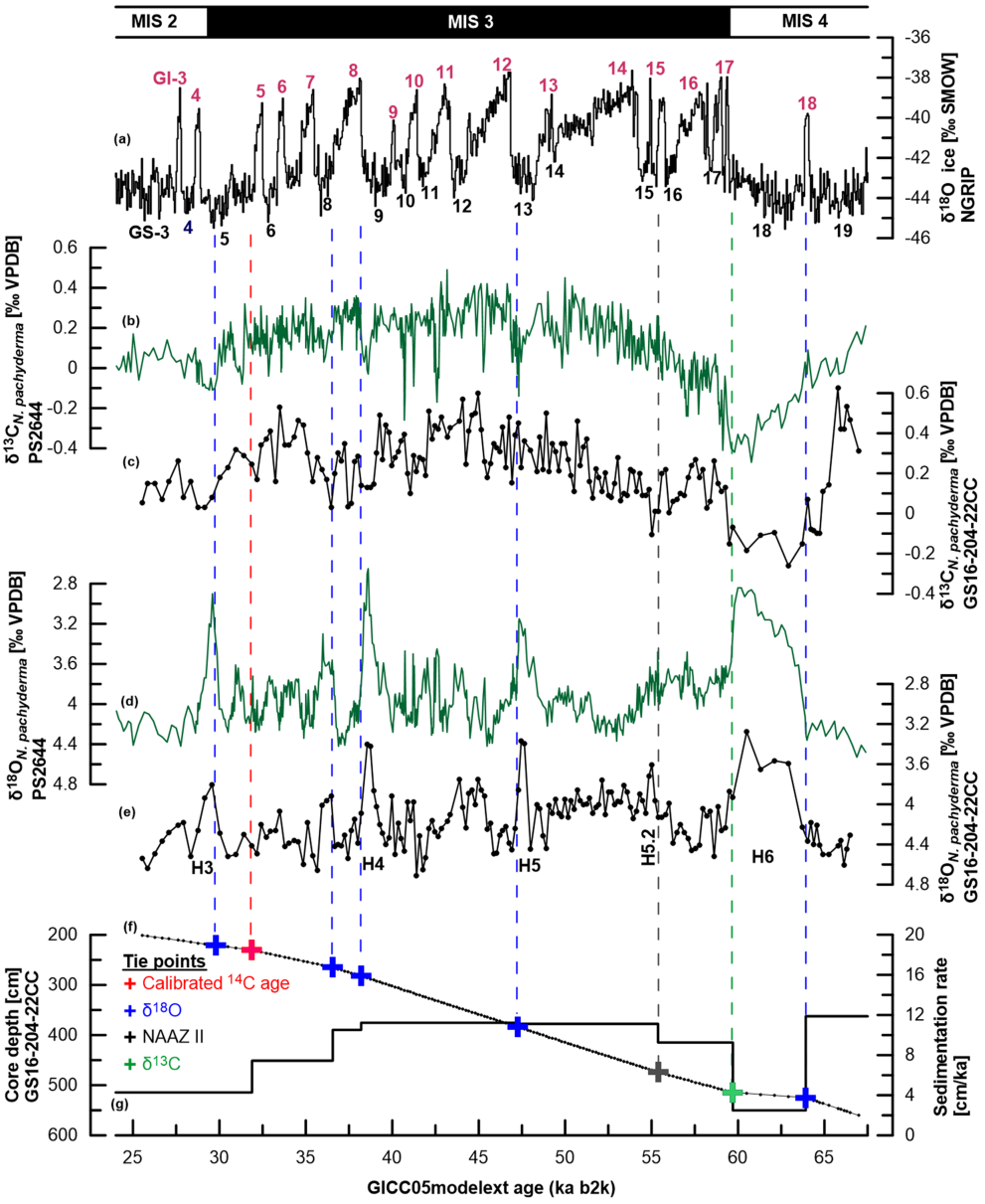

Figure 2. Chronology of core GS16-204-22CC and PS2644-5 (Voelker & Haflidason, 2015a, adjusted to b2k by adding 50 years; Voelker & Haflidason, 2015b) on ka b2k age scale. (a) $\delta^{18}O$ of the NGRIP ice core (Seierstad et al., 2014) with indicated Greenland interstadials (GI, red) and Greenland stadials (GS, black). (b) Planktic $\delta^{13}C$ data of core PS2644-5. (c) Planktic $\delta^{13}C$ data of core GS16-204-22CC. (d) Planktic $\delta^{18}O$ record of core PS2644-5. (e) Planktic $\delta^{18}O$ record of core GS16-204-22CC. (f) Tie-points on age-depth plot: Calibrated ^{14}C age (red cross), $\delta^{18}O$ (blue crosses), North Atlantic Ash Zone (NAAZ) II (gray cross) and $\delta^{13}C$ (green cross). (g) Corresponding sedimentation rates. H3-H6 indicate the corresponding time periods of the depleted $\delta^{18}O$ values.

decreased iceberg discharge or reduced melting, an ice-free ocean or when melting ice does not transport a large amount of coarse debris.

The number of foraminifers consists of benthic and planktic foraminifer tests. The planktic foraminifer abundance (number/g dry sediment) is used as a proxy for sea surface productivity. It is driven by the thickness and extent of the local sea-ice cover controlling the supply of light and nutrients. The highest planktic foraminifer abundances are characteristic for the sea-ice edge, polynyas or large icebergs (e.g. Kohfeld et al., 1996; Ramseier et al., 2001; Smith et al., 2007). Ice-free areas off the sea-

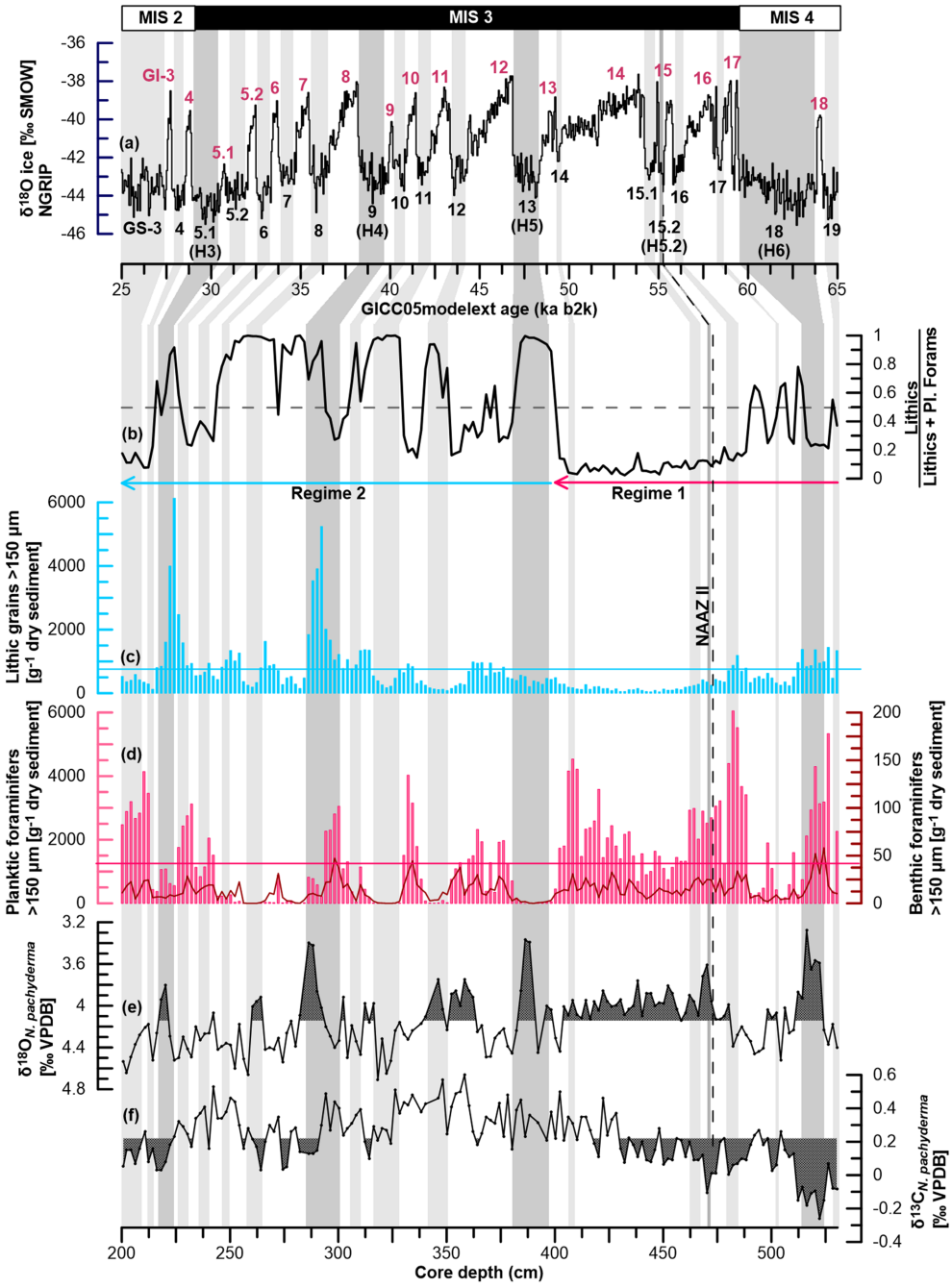

Figure 3. Proxy data of GS16-204-22CC-A versus core depth (bottom) and time (top). All Greenland stadials (GS) are indicated in grey, with a darker grey emphasis on H-associated GS H3-H6. (a) $\delta^{18}O$ of the NGRIP ice core (Seierstad et al., 2014) with indicated Greenland interstadials (GI, red) and GS, (black). (b) Lithics*(Lithics + planktic foraminifers)$^{-1}$ (black), horizontal dashed line indicates the transition between lithic and foraminifer dominated time periods leading to the subdivision of regime 1 and 2. (c) Lithic grain concentration per gram, the blue line indicates the average amount of total IRD. (d) Planktic (pink) and benthic (dark red) foraminifer concentration per gram, the pink line indicates the average amount of total planktic foraminifer concentration. (e) $\delta^{18}O$ of planktic species *N. pachyderma*, filling indicates values lower than the overall average. (f) $\delta^{13}C$ of planktic species *N. pachyderma*, filling indicates values lower than the overall average.

ice margin can also be characterized by high concentrations of planktic foraminifers whereas a perennial sea-ice cover or a lack of nutrients would lead to the absence of planktic foraminifers (Dowdeswell et al., 1998).

Fluxes were calculated by multiplying the respective concentrations with the bulk mass accumulation rate following Peck et al. (2007). Sediment particle, carbonate and water densities of 2.650, 2.730 and 1.025 g cm^{-3} were assumed, respectively. Sedimentation rates used to calculate bulk mass accumulation rates for cores PS2664-5 and SU90-24 were derived from the updated GICC05 related age models, respectively (see subchapter 4, Chronology). The ratio between lithic grains and planktic foraminifers was calculated using the following equation: lithic grains * (total entities)$^{-1}$ (Bond et al., 1992; Heinrich, 1988).

Planktic foraminifer assemblage counts in the 150-500 μm size fraction were performed for 31 samples, spread irregularly through the studied section. Each sample was split until a minimum of 300 specimens was left for counting. The results are given as percentage *N. pachyderma* (%Np). %Np between 90 and 94 % represents the movement of the arctic front whereas values between 94 and 98 % are representative for the location of the polar front (Pflaumann et al., 1996). The fronts divide the North Atlantic into Polar, Arctic and Atlantic waters. Due to the increasing water temperatures, the %Np declines in the direction of Atlantic water (Johannessen et al., 1994).

4. Chronology

The AMS ^{14}C ages below 371 cm are outside of the calibration range (Table 1) and it is known that the reservoir ages of the AMS ^{14}C ages >10 ka BP are highly variable during the glacial period in this region (e.g. Sarnthein et al., 2001; Sarnthein et al., 2015; Waelbroeck et al., 2001) Consequently, we followed a different approach to establish a chronostratigraphy for 22CC. For the final age model, we combined three different types of control points (Figure 2, Table 2). The stratigraphy between 15 and 32 ka b2k is mostly based on two of the calibrated AMS ^{14}C dates, whereas the North Atlantic Ash Zone (NAAZ) II tephra layer provides an independent age control point in early MIS3. NAAZ II (55.38 ± 1.184 ka b2k) is a very well-known volcanic horizon recorded in both marine sediment cores from the North Atlantic (Austin et al., 2004 and references therein) and in Greenland ice cores (e.g. Svensson et al., 2008).

To create a more detailed chronology during MIS3 and MIS4 for core 22CC (Figure 2), we synchronized the planktic $\delta^{18}O$ and $\delta^{13}C$ time series between 22CC and core PS2644-5 (Voelker & Haflidason, 2015a) following Jansen (1989), using the program AnalySeries (Paillard et al., 1996). Core PS2644-5 (hereafter PS2644) was retrieved from the Greenland Sea, off Northwest Iceland (67°52.02'N, 21°45.92'W, 777 m water depth), and has a well constrained chronology based on tuning between the planktic $\delta^{18}O$ and the ice core GISP2 $\delta^{18}O$ record (GISP2 ages converted to GICC05, Voelker & Haflidason, 2015a). The tuning approach is supported by independent time markers including AMS ^{14}C dates, tephra horizons and geomagnetic data (Voelker et al., 1998; Voelker et al., 2000; Voelker & Haflidason, 2015a).

The synchronization between 22CC and PS2644 is based on three assumptions. First, we assume that the near-surface oceanographic changes at the two sites occur virtually synchronously with regard to the age resolution of the cores. Second, the $\delta^{18}O$-depletions are believed to represent large meltwater fluxes occurring during Greenland stadials associated with H-events (hereafter indicating the temporal association, not the character, of a H-event). It is further assumed that the changes in surface water-mass properties are influenced by the same surface currents, in particular the EGC and the Irminger Current.

Finally, seven visually tuned tie-points were used for the synchronization between 22CC and PS2644 (Table 2 and Figure 2). The $\delta^{13}C$ tie-point constrains the sharp MIS4/3 transition whereas the $\delta^{18}O$ tie-points were added to tune the depleted $\delta^{18}O$ peaks to the H-events recorded in PS2644. Sedimentation rates vary between ~2.5 and 12 cm/ky with the highest values occurring prior to H6 and during the middle of MIS3, and the lowest values occurring during H6 and MIS2 (Table 2 and Figure 2).

For this study, the age model of SU90-24 (Elliot et al., 1998) was updated using the IntCal13 calibration curve (Reimer et al., 2013), tuned to the GICC05 age scale (Voelker, 2018) and adjusted to b2k by adding 50 years.

The age-depth relationship of the final age model is shown in Figure 2f. Positive age offsets between the calibrated ages and the ages of the final age model are assumed to reflect the magnitude of contamination (Table 1). Negative age offsets of up to 1.92 ka (+405 years) might indicate a closed sea-ice cover similar to age offsets previously reported for the Younger Dryas and other cold events (e.g. Bard et al., 1994; Sarnthein et al., 2015; Waelbroeck et al., 2001). The measured ^{14}C ages are not in a stratigraphic order from 410 cm downwards.

5. Results

5.1. Lithic Grain and Foraminifer Abundances

On average, the sediment samples contain 689 lithic grains (45 to 6133 grains/g), 1385 planktic (0 to 6048 specimens/g) and 14 benthic foraminifers per gram (0 to 58 specimen/g) in the >150 μm size fraction (Figure 3). The concentrations of benthic and planktic foraminifers follow a similar trend. The lithic/(lithic+foraminifer) ratio shows that planktic foraminifers dominate the sediment between 530 cm and 400 cm (Figure 3). From 400 cm upwards, lithic grains dominate Greenland stadials whereas planktic foraminifers are dominant during Greenland interstadials, albeit with a generally increasing contribution of lithic grains from 315 cm to 240 cm and during H3. Before and after H3, planktic foraminifers are more abundant than lithic grains. Volcanic grains were counted separately in order to detect tephra horizons. We observe one pronounced tephra peak independent of the lithic grain concentration at 474 cm depth. This horizon contained mostly transparent rhyolitic tephra shards corresponding to NAAZ II. The calculated fluxes (Figures 4 and 5) generally follow the above trends; only during H6 (514-524 cm) and H3 (218-220 cm) the foraminifer and IRD signals are smeared out due to the low sedimentation rates.

The planktic foraminifer assemblages are dominated by *N. pachyderma* with minor occurrences of *Neogloboquadrina incompta*, *Turborotalita quinqueloba, Globigerina bulloides, Globigerinita glutinata* and *Globigerinita uvula*. The lowest %Np values (95.1%, 92.7% and 93%) were observed corresponding to Greenland interstadials at ~52.5 ka b2k, ~45.7 ka b2k and ~37.7 ka b2k, respectively (Figures 4 and 5).

5.2. Stable Isotope Data

The stable oxygen isotope record shows three distinct $\delta^{18}O$ depletions at Greenland stadials coinciding with H6, H5 and H4. These depletions have values of ~3.47 ‰, ~3.38 ‰ and ~3.41 ‰, respectively (Figures 2 and 3). The $\delta^{18}O$ signals with values lower than the recorded average (4.15 ‰) indicate additional minima from ca. 480-400 cm, 365-340 cm, 314 cm, 302 cm, 262 cm and 222 cm (H3). Each of these minima is followed by a rapid switch to heavier $\delta^{18}O$ values by up to 1 ‰. Maximum values of 4.71 ‰ are recorded from 316-324 cm resulting in an overall amplitude of up to 1.33 ‰.

The stable carbon isotope record shows an average $\delta^{13}C$ value of 0.22 ‰ (Figure 3). The lowest $\delta^{13}C$ values are observed during the three depth intervals corresponding to low $\delta^{18}O$ values, from ca. 530-430 cm (including H6), 290-262 cm (including H4) and 225-200 cm (MIS2), with the most pronounced minimum coinciding with H6 (-0.26 ‰). Maximum values of 0.51 to 0.60 ‰ occur during MIS3. In general, the $\delta^{13}C$ record seems to show lower values during Greenland stadials.

6. Discussion

The relationship between the abundance of lithic grains (hereafter IRD) and planktic foraminifers (Figure 3) leads to a subdivision of the 22CC records into two different regimes. Regime 1 spans from approximately 65 to 49 ka b2k and is characterized by an overall dominance of planktic foraminifers in the coarse fraction (>150 μm) compared to the IRD content. During regime 2 (~49-25 ka b2k), a generally higher flux of IRD is observed with specific IRD events marked by an IRD content nearly one order of magnitude higher than the rest of this period. The abundance of planktic foraminifers during regime 2 is highly variable, from almost barren in some intervals to relatively high amounts in others. This "on and off" signal in foraminifer abundance seems to oscillate on millennial timescales related to abrupt climate oscillations recorded in Greenland ice cores. After the proxy records of 22CC are discussed, the 22CC records will be set into a regional context by comparing them with proxy records from the Greenland Sea (PS2644, Voelker et al., 1998) and from the Irminger basin (SU90-24, Elliot et al., 1998) on the basis of the Greenland stadial/interstadial (GS/GI) changes.

In the following discussion we use some general characteristics for subdividing the studied period and interpreting the environmental conditions:

- As foraminifer production and flux in the polar region is highly influenced by food availability, an extensive sea-ice cover in the polar region and its associated limited light penetration, is the primary influence leading to reduced fluxes (Carstens et al., 1997; Kohfeld et al., 1996; Ramseier et al., 2001). Hence, as light

and nutrients are limited below sea-ice, the foraminifer flux can be used as a proxy for sea-ice cover changes (Greco et al., 2019). Oceanic frontal processes provide an increased nutrient supply and enhanced productivity although they are also linked to the extent of the summer (polar front) or winter (arctic front) sea-ice cover (Johannessen et al., 1994). The salinity changes induced by meltwater derived from a melting sea-ice cover also affect planktic foraminifer production and their habitat depth.

- The flux of IRD is primarily influenced by iceberg supply and iceberg melting rates. A dense sea-ice cover inhibits iceberg transport and reduces IRD flux, whereas the associated cold surface waters cause lower melt rates. Warmer waters enhance melting and IRD flux (e.g. Straneo & Heimbach, 2013), if the melting icebergs still contain sediment that can be dropped.
- Sedimentation rates over the Eirik Drift are highly variable. During interglacials the Deep Western Boundary Current was active at the depth of the core, leading to enhanced sedimentation of fine material and dilution of coarse-grained particles (Hillaire-Marcel et al., 1994; Hillaire-Marcel et al., 2011; Stoner et al., 1998). During glacial times, on the other hand, the boundary current was less active and shallower, leading to reduced dilution. Hence, the primary control of IRD concentration and calculated fluxes are taken to be a combination of iceberg supply and melt rates.

6.1. GS/GI Oscillations During Regime 1: Stable Climates During a Sea-Ice Covered vs. Open Northeastern Labrador Sea

Regime 1 is defined by overall very low IRD fluxes and can be divided into two sub-intervals; A) the older sub-interval spanning late MIS4 across the MIS4/3 transition to GI-17.2 to GI-16; and B) the younger sub-interval encompassing the interval from GI-16 to GI-13 (Figure 4). The older sub-interval is characterized by relatively low foraminifer fluxes, a shift from depleted (GS-18) to high $\delta^{18}O$ values (MIS4/3 transition) and %Np values around 98 %. Values between 98 and 94 % of *N. pachyderma* in the planktic assemblage are associated with the location of the oceanic polar front nearby which likely represents the extent of the summer sea-ice, as known from the Nordic Seas (Johannessen et al., 1994; Pflaumann et al., 1996). Today, the polar waters along the East-Greenland margin are dominated by the EGC which exports icebergs and sea-ice from the Arctic Ocean and Nordic Seas. South of the Denmark Strait, the polar waters are seasonally sea-ice free allowing for plankton productivity. Combining the %Np data and the foraminifer flux we interpret that our core location was covered by near-perennial sea-ice during the older part of regime 1 although a few icebergs were transported by the EGC which discharged some IRD. Although the foraminifer and IRD concentrations are high (Figure 4) the very low sedimentation rates smear those signals out in terms of their flux. Low sedimentation rates probably reflect a closed sea-ice cover, which limited vertical particle flux and iceberg transport (Dowdeswell et al., 1998). It might also be indicative for times with a weak boundary current at the depth of the site. The enhanced Arctic freshwater export by the EGC associated with H6, indicated by the depleted $\delta^{18}O$ values, could be another reason for the lower surface productivity and hence relatively low foraminifer flux. Just before and after the H6 meltwater peak (GI-18 and GI-17), the 22CC foraminifer flux increases to moderate levels when the $\delta^{18}O$ values increase, apparently as a result of diminished freshwater input. *N. pachyderma* is thought to adjust its depth habitat following the pycnocline and hence inhabits greater depths during conditions of increased freshwater supply or sea-ice (Greco et al., 2019;Pflaumann et al., 2003 ; Simstich et al., 2003). We exclude the possibility of lower fluxes due to sediment export or erosion since we expect bottom currents to be weaker during this glacial period as the thermohaline circulation was also reduced during H6 (Böhm et al., 2015; Hunter, Wilkinson, Louarn, et al., 2007; Rahmstorf, 2002). Thus, the variability of foraminifer fluxes during MIS4 and at the MIS4/3 transition can primarily be attributed to the variable influence of sea-ice and freshwater (e.g. Dokken et al., 2013; Hillaire-Marcel et al., 2011) related to the GI/GS shifts during the older sub-interval of regime 1.

The H6 freshwater signal is also recorded in cores PS2644 and SU90-24, confirming our interpretation of enhanced Arctic freshwater export (e.g. Elliot et al., 1998; Voelker et al., 1998). While the %Np values are similar in 22CC and PS2644, the foraminifer fluxes are lower and the IRD flux is higher in the Greenland Sea throughout the older part of regime 1. The lower foraminifer flux might suggest an extensive sea-ice cover for most of the year in the Greenland Sea in line with independent sea-ice reconstructions by De Schepper et al. (2019). The generally higher IRD flux in core PS2644 is most likely caused by material transported by icebergs with a possible admixture of material transported by sea-ice from coastal areas. Icebergs would contain eroded material from the East-Greenland fjords, Iceland (Andrews et al., 2017) or possibly the

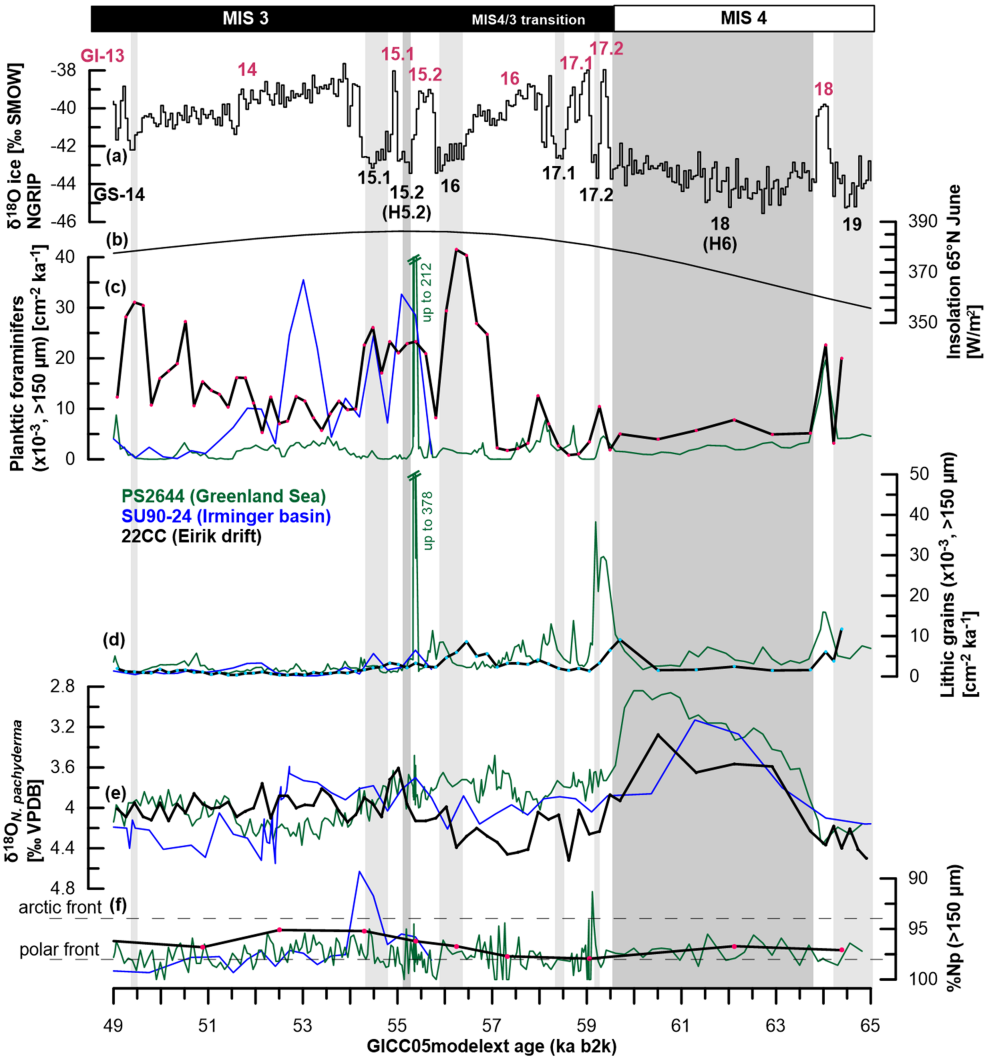

Figure 4. Surface proxy data for sediment regime 1 of core GS16-204-22CC-A (this study, black lines), PS2644 (Greenland Sea, green (Voelker & Haflidason, 2015a; Voelker & Haflidason, 2015b)) and SU90-24 (Irminger basin, blue (Elliot, 2017; Elliot et al., 1998; on modified age model)) versus GICC05 age. All data were adjusted to the b2k scale by adding 50 years. All Greenland stadials are highlighted in grey with a darker grey emphasis on H-associated Greenland stadials (GS) H6 and H5.2. (a) $\delta^{18}O$ of the NGRIP ice core (Seierstad et al., 2014) with indicated Greenland interstadials (GI, red) and Greenland stadials (black). (b) Solar insolation 65°N for June (Laskar et al., 2004). (c) Flux of planktic foraminifers >150 µm. (d) Flux of lithic grains >150 µm. (e) $\delta^{18}O$ of planktic species *N. pachyderma*. (f) %Np indicating the influence of warmer Atlantic water, dashed lines highlight values indicating the oceanic polar front (~98%) and arctic front (<94%) according to Pflaumann et al. (1996).

Eurasian shelf (Stein et al., 1996) as the Fennoscandian ice sheet was well established during MIS4 (Svendsen et al., 2004 and references therein). The IRD event immediately at the onset of MIS3 in PS2644 may have been caused by retreat of the extensive Arctic sea-ice cover which allowed for higher iceberg supply/melt rates, potentially in combination with influx of warmer subsurface waters as observed at the Faeroe Shetland ridge at this time (Ezat et al., 2014). A decrease of %Np (at ~59 ka b2k), following the IRD event, indicates the advection of warmer Atlantic water influenced the site in the Greenland Sea (Figure 4). However, neither the sharp IRD peak nor the higher influence of Atlantic water in PS2644 is recorded by 22CC, indicating a more limited invasion of these waters south of Greenland.

The second part of regime 1 commenced with a sharp increase in foraminifer flux during GI-16 while the IRD fluxes remained minimal and the $\delta^{18}O$ values were quite stable. The foraminifer fluxes reach the highest

values of the entire 22CC record between GI-16 and GI-13 indicating highly productive surface waters. Most likely, the northeastern Labrador Sea was characterized by open-water conditions for most of the year during this time interval. This might have been caused by the solar insolation maximum and consequent warmer atmospheric temperatures during GI-14. The %Np values also reflect slightly warmer sea surface temperatures within the limits of the polar front. When the %Np values are closest to 94% (GI-14), representing the location of the arctic front and hence the winter sea-ice edge, the 22CC foraminifer flux decreased to moderate levels. This might indicate that the EGC shifted closer towards the Greenland continental margin causing an increased influence of the Irminger Current in the northeastern Labrador Sea. In line with this interpretation, several published studies from the North Atlantic note a subsurface warming due to a stronger advection of the North Atlantic Current for GI-14 (e.g. Barker et al., 2015; Hillaire-Marcel et al., 2011; Lackschewitz et al., 1998; Naafs et al., 2013; van Kreveld et al., 2000). Hence, the diminished influence of sea-ice along with decreased nutrient supply and frontal mixing might have reduced food availability from phytoplankton sources (e.g. Belt et al., 2007; Ramseier et al., 2001). Today, *N. pachyderma* represents ca. 95% of the planktic foraminifer assemblage at the Eirik drift and lives in water depths between 70 and 130 m below the EGC (Pflaumann et al., 2003; Simstich et al., 2003) while the polar front is located north of our core site (Yashayaev et al., 2015). Present day conditions correspond well with our interpretations for GI-14. It has been shown that icebergs from fjords in West and East Greenland reached the Eirik drift during the Holocene (White et al., 2016), supporting our hypothesis that environmental conditions during GI-14 might have been similar to Holocene interglacial conditions in the northeastern Labrador Sea.

The %Np values recorded by PS2644 and SU90-24 remain above those of 22CC, except for one peak at ~54.2 ka b2k in SU90-24, representing the higher influence of the EGC at those locations. But, while PS2644 records low foraminifer fluxes and hence an extensive near-perennial sea-ice cover in the Greenland Sea, the foraminifer fluxes recorded in the Irminger basin reach the same levels as in 22CC or even exceed them, for example during GS-15.2 and in parts of GI-14. Core PS2644 also records a peak in foraminifer flux during GS-15.2, accompanied by a sharp peak in IRD flux, which might be related to conditions following the volcanic eruptions of NAAZ II (e.g. Frogner et al., 2001). The peak in foraminifer flux during GI-14 in SU90-24 might indicate the higher food availability due to the higher influence of sea-ice, either at the summer sea-ice edge or exported by the EGC, compared to our core site. Additionally, the very low IRD input during GI-14 seems to be a phenomenon in wide parts of the North Atlantic basin (e.g. Barker et al., 2015; Elliot et al., 1998; Hagen & Hald, 2002; Hillaire-Marcel et al., 2011; Lackschewitz et al., 1998; van Kreveld et al., 2000; Voelker et al., 1998).

In summary, our proxy records show similar trends with those recorded by the Greenland ice cores for regime 1, specifically the colder climate conditions during MIS4 shifting towards a warmer climate without DO-like temperature oscillations on millennial-scale (GI-14 to GI-13) (Huber et al., 2006; Seierstad et al., 2014). Until GI-16, the summer sea-ice edge (and polar front) was close to the study site. Thereafter, it retreated northwards while the high plankton productivity was maintained by melt of the sea-ice after the winter months. The slightly warmer sea surface temperatures, very low iceberg activity and high productivity in the northeastern Labrador Sea during GI-14, suggests environmental conditions similar to Holocene conditions. These may have been caused by the solar insolation maximum at that time. In contrast, an extensive, near-perennial sea-ice cover was maintained in the Greenland Sea.

6.2. GS/GI Oscillations During Regime 2: High Variability of Environmental Conditions

Regime 2, which covers the younger half of MIS3 and the beginning of MIS2 (GS-13 to GS-3, Figure 5), shows large variability in all analyzed proxies that in part appear to be related to the GI/GS oscillations recorded by the Greenland ice cores. The $\delta^{18}O$ record exhibits notably pronounced excursions to strongly depleted values during GS-13 and GS-9, corresponding to the North Atlantic H-events H5 and H4, respectively. Additional time periods with pronounced low values are the younger part of GI-12, GS-12, GS-8 and GS-5.1 (H3). In association with the strongly depleted $\delta^{18}O$ values, %Np are lower than 94% in GI-12 and GI-8 which follow H5 and H4. The planktic assemblages in GI-12 and GI-8 of 22CC reveal an increased number of subpolar species *T. quinqueloba* and *G. bulloides* indicating the presence of warm Atlantic water. The lower %Np might indicate a temperature increase in the subsurface as suggested for the Greenland Sea, Fram Strait, central North Atlantic and Nordic Seas (e.g. Dokken et al., 2013; Knutz et al., 2011; Rasmussen & Thomsen, 2004; Voelker et al., 1998). It seems likely that the advection of warm Atlantic water was enhanced facilitating

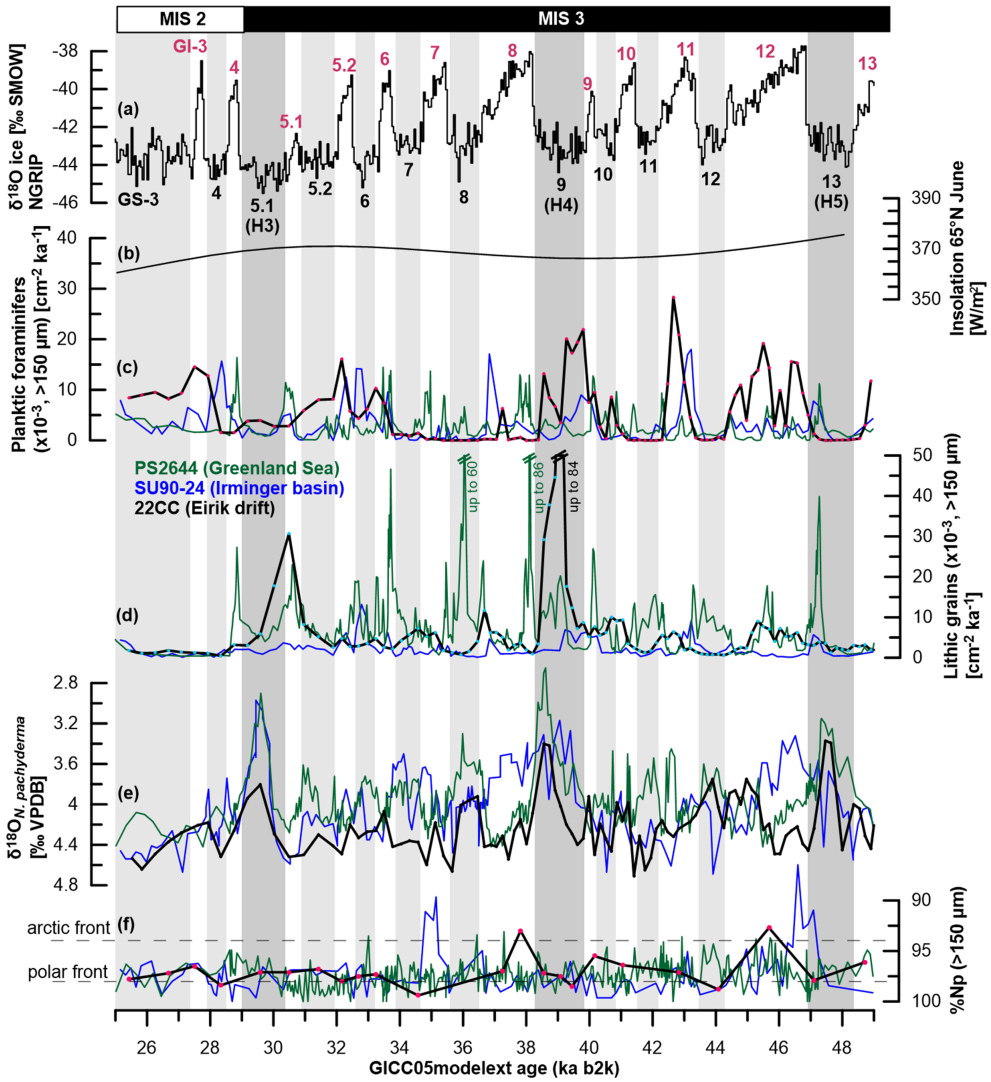

Figure 5. Surface proxy data for sediment regime 2 of core GS16-204-22CC-A (this study, black lines), PS2644 (Greenland Sea, green (Voelker & Haflidason, 2015a; Voelker & Haflidason, 2015b)) and SU90-24 (Irminger basin, blue (Elliot, 2017; Elliot et al., 1998; on modified age model)) versus GICC05 age. All data were adjusted to the b2k scale by adding 50 years. All Greenland stadials are highlighted in grey with a darker grey emphasis on H-associated Greenland stadials (GS) H5 to H3. (a) $\delta^{18}O$ of the NGRIP ice core (Seierstad et al., 2014) with indicated Greenland interstadials (GI, red) and Greenland stadials (black). (b) Solar insolation 65°N for June (Laskar et al., 2004). (c) Flux of planktic foraminifers >150 µm. (d) Flux of lithic grains >150 µm. (e) $\delta^{18}O$ of planktic species *N. pachyderma*. (f) %Np indicating the influence of warmer Atlantic water, dashed lines highlight values indicating the oceanic polar front (~98%) and arctic front (<94%) according to Pflaumann et al. (1996).

the reestablishment of the thermohaline circulation patterns (Mignot et al., 2007) after the reduced mode that might have occurred due to the large freshwater input during H-events (Böhm et al., 2015; Rahmstorf, 2002). Apart from those two excursions the %Np values, where this proxy could be applied, stay within or above the values defining the location of the polar front indicating seasonally open waters with the EGC as the dominant surface current.

During most GSs of regime 2, the %Np proxy could not be applied because foraminifer abundance is too low. This is also reflected in the foraminifer fluxes which show large variability in regime 2. All time periods where foraminifers are nearly absent in the coarse fraction, tend to fall within GSs, although some of those periods extend into GIs (GI-8, GI-7). We argue that during those time periods our core location was covered by near-perennial sea-ice. During periods of minimum foraminifer flux, IRD flux is also reduced, which might indicate that a thick sea-ice cover prevented icebergs from entering the area or cold surface temperatures inhibited melt-out from icebergs. The higher $\delta^{18}O$ values observed during many GSs in core 22CC are

Table 2
Age Control Points in Sediment Core GS16-204-22CC-A Used for the Established Chronology

Pointer based on:	Depth (cm)	Age of tie point (ka b2k)	Sedimentation rate (cm/ky)
AMS ^{14}C	150.5	15.09	4.8
δ^{18}O	221.5	29.79	4.3
AMS ^{14}C	230.25	31.89	7.4
δ^{18}O	265.00	36.56	10.5
δ^{18}O	282.25	38.2	11.2
δ^{18}O	384.00	47.26	11.1
Ash layer (NAAZ II[a])	474.25	55.38	9.3
δ^{13}C	514.25	59.7	2.5
δ^{18}O	524.75	63.92	11.9
δ^{13}C	604.5	70.64	11.9

[a]55.38 ± 1.184 (NGRIP; Svensson et al. (2008))

consistent with a reduced meltwater influence in the northeastern Labrador Sea (Figure 5). Extensive sea-ice cover throughout most of the year would prevent light penetrating the water column and reduce primary production, leading to limited food availability for the planktic as well as benthic foraminifers. Thus, the sea-ice edge was probably located south of our site accompanied by a southward expansion of the EGC. The short increase in foraminifer flux occurring simultaneously with the low %Np value during the sea-ice covered GI-8 might indicate the opening of a polynya caused by the northward advected Atlantic water which could have triggered an increase in plankton production (e.g. Duprat et al., 2016; Smith et al., 2007; Stern et al., 2015; Vettoretti & Peltier, 2016). Vettoretti and Peltier (2016) found that a North Atlantic polynya could have appeared at the onset of each DO-warming event during wintertime. Low light conditions during winter could explain why the foraminifer flux during GI-8 increased, albeit to low levels. Although dissolution due to more corrosive bottom waters cannot be completely excluded, the foraminifers that we find in these low flux time periods appear pristine. Additionally, the sediment deposited at this time at site 22CC is dominated by the fine fraction, which strongly implies an extensive, near perennial sea-ice cover and a weak bottom current. At the end of GI-8, following the increased foraminifer flux peak and the low %Np, the IRD flux increases, confirming that conditions changed above our core site. In particular, the break-up of the sea-ice cover is likely, and allowed for the passing (and melting) of icebergs and potentially the (subsurface) influx of the Atlantic waters. Observations at core sites CH69-K09 (southeast of Newfoundland, Labeyrie et al., 1999) and SO82-05 (Reykjanes ridge, van Kreveld et al., 2000) suggest an influx of warm waters at the end of GI-8; these observations support our interpretation, assuming the warmer waters reached the northeastern Labrador Sea. Similar conditions probably occurred during GS-10 when foraminifer fluxes also increase accompanied by moderate IRD fluxes and lower %Np values.

Moderate to high foraminifer fluxes are mainly recorded during GIs of regime 2 as well as during GS-9 (H4), GS5.2 and GS-3. While the GSs of the older part of regime 2 are characterized by a near-perennial sea-ice cover, the seasonally open water conditions during the GIs allow for iceberg transport as well as higher productivity and food availability for the foraminifers. Different mechanisms must have driven the environmental conditions in the younger part of regime 2 (GS-9, GI-7 to GS-3) because foraminifer and IRD fluxes are no longer in phase. Instead, the foraminifer fluxes are higher when the IRD fluxes are lower and vice versa.

In time periods with high δ^{18}O values, low foraminifer fluxes and increased IRD fluxes (middle of GS-9, end of GI-8, GS-7, GI-5.1 into GS-5.1) during regime 2, iceberg activity could have had a negative impact on foraminifer productivity (similar to that observed in the Southern Ocean; Schwarz & Schodlok, 2009). A high number of melting icebergs may cause water column stratification with a meltwater lid forming at the surface. The planktic foraminifers would be expected to follow the pycnocline to greater water depths were the food availability (or quality) might have been limited. We suggest that this explanation is sufficient for the high numbers of icebergs reaching our site associated with the H4 and H3 calving events, but this does not necessarily explain the increase of IRD fluxes between H4 and H3 (end of GI-8, GS-7). Here we suggest that sea surface conditions were not favorable for plankton blooms. The IRD flux likely represents iceberg transport via the EGC, and not any particular calving events.

The $\delta^{18}O$ values are high while the foraminifer fluxes are increased, and the IRD fluxes are low at the beginning of GS-9, from GI-6 to GS-5.2 and GI-3 to GS-3. One possible explanation could be that although the sea-ice retreated during the summer months and iceberg transport routes were free, melting was hampered by very cold surface waters. A cold and seasonally ice-covered northeastern Labrador Sea from 31 ka was also reported from a dinocyst and coccolithophore study (Rahman & de Vernal, 1994). On the other hand, melting starts with water temperatures around 0°C and our %Np values do not indicate especially cold temperatures compared to intervals where iceberg melting occurred. Other explanations could be that either polynyas developed in the area that allowed plankton productivity (e.g. Duprat et al., 2016; Ramseier et al., 2001; Schwarz & Schodlok, 2009; Smith et al., 2007; Stern et al., 2015) or that icebergs passing the site during the given time periods transported less sedimentary material. Additionally, the increasingly high $\delta^{18}O$ values recorded in core 22CC during regime 2 incorporate the signal of the increasing global continental ice volume towards the last glacial maximum. Global benthic isotope records as well as models show that sea level was dropping from ~32 ka until it reached its minimum around 21 ka while ice sheets reached their maximum volumes at ~30 ka and remained constant until ~19 ka (Clark & Mix, 2002; Lambeck et al., 2002; Waelbroeck et al., 2002). Hence, fewer icebergs might have been discharged between 30 to 19 ka due to a stable mass balance and a near-perennial sea-ice cover in the Greenland Sea and the Arctic Ocean (De Schepper et al., 2019; Patton et al., 2016).

To evaluate the transport of icebergs and freshwater by the EGC during regime 2, we again compare the records from our core site (22CC) to the proxy records from the Greenland Sea (PS2644, Voelker et al., 1998) and the Irminger Basin (SU90-24, Elliot et al., 1998). We observe that the SU90-24 records are more similar to our data than those of PS2644 (Figure 5), particularly the trends in the foraminifer fluxes. Apparent temporal offsets between core SU90-24 and 22CC are most likely caused by the uncertainty of the age models rather than climatic conditions. IRD fluxes at site SU90-24 stay low during regime 2, but are synchronously coupled to the increase in the foraminifer fluxes during GIs. Elliot et al. (1998) explain this by invoking rapid fluctuations in sea-ice extent, leading to seasonal sea-ice edge conditions resulting in increased IRD flux and sea surface productivity. This explanation has been promoted by several other studies (e.g. Bond, 1997; Johannessen et al., 1994; Ramseier et al., 2001) and corresponds well with our interpretation for most GIs of regime 2.

The %Np data of SU90-24 are also similar to that recorded in 22CC (Figure 5) and indicate a proximal location of the polar front and hence the summer sea-ice edge. Exceptions to this overall trend occur during GI-12 (as in 22CC) and GI-7, indicating subsurface warming and possibly a longer sea-ice free season throughout the year. During GI-12 the low %Np values are accompanied by low $\delta^{18}O$ values in core SU90-24 which contradicts the high $\delta^{18}O$ values observed in 22CC. Those differences could be explained by different calcification depths of *N. pachyderma* related to local sea-ice cover, meltwater lenses or isotopically light brines (Hillaire-Marcel et al., 2011; Simstich et al., 2003). Unexpectedly, neither the inferred warm water nor the freshwater flux changes seem to affect the IRD and foraminifer fluxes which stay low at site SU90-24. Similar to SU90-24, core SO82-05 (Figure 1) also records low $\delta^{18}O$ values during GI-12 and GI-7 associated with increasing sea surface temperatures and salinities, clearly indicating the higher influence of Atlantic water during those GIs (van Kreveld et al., 2000). This hypothesis is further supported by benthic isotope records and chemical water tracers indicating the return to well-ventilated deep waters and thus an active thermohaline circulation during the GIs following H-events (Böhm et al., 2015; Elliot et al., 2002; Henry et al., 2016; Labeyrie et al., 1999; van Kreveld et al., 2000). The activated deep and surface water circulation could also have influenced the hydrography of the Labrador Sea. Hence, the high $\delta^{18}O$ values recorded by 22CC could reflect a salinity signal as the result of an active subpolar gyre circulation while site SU90-24 was mainly influenced by the EGC, similar to conditions today.

According to the %Np data, PS2644 is not influenced by Atlantic water advection but records shifts of the polar front. Foraminifer fluxes are lower in PS2644 compared to site 22CC, but they also increase during most GIs and drop during most GSs (Figure 5). Interestingly, foraminifer fluxes also increase between GI-8 and GS-7, whereas foraminifers are nearly absent in SU90-24 and 22CC. In the same time period, besides the peak at the end of GS-13, PS2644 records three very pronounced peaks in IRD fluxes right after H4, during GS-8 and GI-6 indicating significant calving events north of the Denmark Strait, contrary to conditions south of the Denmark Strait.

Table 3
Summary of Characteristics of Heinrich Events 3-6 in Core GS16-204-22CC

Heinrich event	Approximate age (ka b2k)	Planktic $\delta^{18}O$ (meltwater)	IRD flux	Foraminifer flux	Subsurface warming
3	30.3-29.0	Low	High	Low	No
4	39.9-38.2	Depleted	High	Moderate	Yes (GI-8)
5	48.3-46.9	Depleted	Very low	Very low	Yes (GI-12)
6	63.8-59.5	depleted	Very low	Low	No

Apart from the differences caused by local hydrography, all three sites show evidence of a shifting winter sea-ice edge influencing plankton productivity and iceberg transport on GS/GI timescales. Changes on a millennial timescale seem to be quite common in the marine records from the North Atlantic after H5 and north of 55°N, possibly related to their proximity to continental ice sheets (Andrews et al., 1998; Barker et al., 2015; Elliot et al., 2002; Lackschewitz et al., 1998; van Kreveld et al., 2000).

6.3. The H-Associated GSs

The most pronounced IRD layers caused by the collapses of the Laurentide (H5 and H4) and Eurasian (H6 and H3) ice sheets were discovered in the Ruddiman belt (Bond et al., 1993; Grousset et al., 1993; Grousset et al., 2001; Hemming, 2004; Ruddiman, 1977). It is often assumed that the sea-ice cover extended to the northern edge of that belt at 55°N (Dokken et al., 2013; Vettoretti & Peltier, 2016) because the sea-ice edge would have blocked potential northward iceberg movement as well as northward oceanic heat transport making the Ruddiman belt the most suitable region for melting. During H-events the overturning circulation was reduced (e.g. Böhm et al., 2015; Henry et al., 2016; Rahmstorf, 2002) and the restart of the overturning circulation is observed in North Atlantic proxy records as a temperature overshoot indicating the increased advection of warm water (e.g. Dokken et al., 2013; Knutz et al., 2011; Rasmussen & Thomsen, 2004; Sadatzki et al., 2019; Sessford et al., 2018; van Kreveld et al., 2000; Voelker et al., 1998). The glacial surface hydrography of the northeastern Labrador Sea was influenced by Arctic freshwater and Atlantic water and probably iceberg transport and melt from the Laurentide, Eurasian and Greenland ice sheets (Death et al., 2006; Hemming, 2004; Stoner et al., 1998). Consequently, we would expect to observe H-related meltwater peaks associated with increased IRD fluxes and low foraminifer fluxes, followed by a signal of subsurface warming indicating an active surface and deep water circulation. Instead, the only proxy in the analyzed core sections of 22CC that shows clear evidence of all H-events is $\delta^{18}O$, indicating each H-related meltwater event. Only H6, H5 and H3 are associated with low foraminifer fluxes, H4 and H3 with pronounced IRD peaks and H5 and H4 are followed by subsurface warming (Table 3). Following the interpretations of the proxy records from this site, these differences can largely be explained by the specific environmental conditions in which the H-associated GSs of regime 2 and 1 are placed. Accordingly, the core site appears to have been sea-ice covered for most of the year during H6 and H5 while sea-ice conditions during H5.2, H4 and H3 must have been more open based on the moderate foraminifer flux (H5.2 and parts of H4) and/or high IRD flux (H4 and H3). Hence, the source of the meltwater and transport routes to the northeastern Labrador Sea must have been variable. Possible transport mechanisms are 1) via the EGC, which transported meltwater from the Arctic Ocean, the eastern Greenland ice sheet and the Nordic Seas; 2) via the subpolar gyre, which redistributed meltwater from the Eurasian and Laurentide ice sheets and the associated iceberg melt in the Ruddiman belt; and/or 3) via nepheloid layer transport from the Northwest Atlantic Mid Ocean Channel (NAMOC), triggered by the collapse of the Hudson Strait ice stream (Hesse et al., 2004; Hesse & Khodabakhsh, 2017; Rashid et al., 2003a). However, the latter mechanism can most likely be excluded for our core site because it is located outside of the direct Laurentide ice sheet meltwater plume and the influence of the NAMOC (Stoner et al., 1996). In order to discuss the other two scenarios, we again must compare our $\delta^{18}O$ signal to other core sites within the pathways of the EGC or the North Atlantic/Irminger Current (Figure 1). A north to south gradient is clearly apparent from the core sites along the East and South Greenland margins (Figures 4 and 5). Thus, the most depleted $\delta^{18}O$ signal during H-related GSs is always recorded by northernmost core PS2644, suggesting meltwater transport by the EGC and potential local sources from Iceland. However, the $\delta^{18}O$ values of cores PS2644 and SU90-24 show the biggest difference to 22CC during H6 and H3. At the same time, H6 and H3 are the two

events in core 22CC not followed by a subsurface warming signal. This might suggest that within H6 and H3 iceberg transport and any associated melting occurred within the EGC while current transport into the northeastern Labrador Sea might have been limited. Core SO82-05 also records a meltwater signal for H3 but with a smaller amplitude than PS2644 and SU90-24, which might reflect active subpolar gyre transport with a large component of meltwater from the Eurasian ice sheet, as also suggested by IRD provenance studies from the Ruddiman belt (Hemming, 2004 and references therein). Labeyrie et al. (1999) state that polar waters invaded the North Atlantic at the surface down towards the southern limit of the Ruddiman belt. This freshwater lid is thought to have disrupted the North Atlantic surface circulation, decreasing deep-water formation and subsequently ventilation during H-associated GSs as well as regular GSs. Such a scenario is in agreement with the absence of the Deep Western Boundary Current at the Eirik Drift (Hillaire-Marcel et al., 1994). The resumption of good ventilation at core site CH69-K09 did not follow directly after the H-events but was delayed by several hundred years. Labeyrie et al. (1999) explained this delay by the temporal lead of the meltwater signal at high latitudes and the great depth of their core site (>4000 m) compared to e.g. SU90-24 (Vidal et al., 1997).

7. Conclusions

In this study we present high-resolution stable isotope data, IRD and foraminifer abundances and low-resolution planktic assemblage counts from marine core 22CC (Eirik drift, northeastern Labrador Sea), covering the period between ~65 ka b2k and ~25 ka b2k. Our proxy data provide new evidence about the variability of the sea-ice cover at this location as well as surface productivity and iceberg transport during the abrupt climate shifts of MIS3. Core 22CC records both ice sheet and/or sea-ice responses on millennial timescales (>55°N, Cortijo et al., 1995) as well as various characteristics of H-events 6 to 3.

Our interpretation of the proxy data from this site suggests that: (1) from ~67 ka b2k to ~56 ka b2k site 22CC was covered by near perennial sea-ice, limiting surface productivity and iceberg transport, while from ~56 to 49 ka b2k the sea-ice cover retreated northwards due to the solar insolation maximum. (2) From ~49 ka b2k to ~25 ka b2k, this site was covered by near-perennial sea-ice during most GSs which decreased to seasonal sea-ice cover during most GIs. (3) After H3, the Greenland ice sheet´s ice shelf most likely triggered higher productivity. (4) The surface conditions and convection in the northeastern Labrador Sea are driven by regional mechanisms because all recorded H-events are characterized by different environmental conditions. (5) The southern extent and the lateral expansion of the EGC is not restricted to H-associated GSs at the Eirik drift but seems to be characteristic for the investigated time period.

The comparison of three core sites combined (22CC, SU90-24, PS2644) provides insight into mechanisms potentially involved in creating the environmental conditions seen during the studied period of the last glacial period, especially sea-ice cover extent, plankton productivity and iceberg discharge:

- Orbital forcing enhanced early MIS3 warming and a subsequent cooling trend characterized by more sea-ice and iceberg presence towards the last glacial maximum;
- Increased surface productivity and retreat of winter sea-ice during the solar insolation maximum (GI-14);
- Regime 1 was characterized by a more pronounced general presence of subpolar water masses compared to regime 2. In regime 2, subpolar water masses appeared only during short events in the GIs;
- The similarity between the Eirik Drift and Irminger Sea core indicate both a linkage of signals along the EGC and a more active subpolar gyre during warmer periods;
- Enhanced meltwater flux, in particular during GS-18, GS-13, GS-9 and GS-5.1 by the EGC leading to water column stratification, reduced food availability and furthermore weakened deep-water convection and subpolar gyre;
- Subsurface warming and concomitant heat advection to the sea-ice covered areas (GI-12, GI-8) could have resulted in the opening of polynyas, allowing for the restart of thermohaline convection;
- Iceberg calving episodes associated with H-events are recorded, but differ between the different H-events. Outside of the H-events there was a continued flux of icebergs along the EGC;
- Iceberg calving events (H4 and H3) which occurred during the greatest ice sheet extent led to reduced plankton productivity. The calving events as documented by IRD occurred prior to the main meltwater advection ($\delta^{18}O$ signal) to the area.

Acknowledgments

We thank Eivind W. N. Støren for the facilities of EARTHLAB, Dag Inge Blindheim and Ulysses S. Ninnemann for helping with the stable isotope analyses as well as the use of FARLAB. A thankyou goes to the R/V *G.O. Sars* crew for the successful cruise in 2016 where the analyzed core was retrieved. We also thank Mary Elliot for providing the data necessary to calculate the fluxes of SU90-24 and Sevasti E. Modestou for language editing. We appreciate the positive and constructive suggestions from the reviewers which helped to greatly improve this manuscript. The funding for this research was granted by the European Research Council under European Community's Seventh Framework Programme (FP7/2007-2013) ERC grant agreement 610055 as part of the ice2ice project. A. Voelker acknowledges financial support from the Fundação de a Ciencia e a Tecnologia through grants IF/01500/2014 and UID/Multi/04326/2019. The data shown in this publication is available at the Pangaea data base https://doi.pangaea.de/10.1594/PANGAEA.904065. The supporting information provides figures showing foraminifer and IRD concentrations of core sites 22CC, PS2644 and SU90-24 for regime 1 (S1) and regime 2 (S2).

References

Alley, R. B., Andrews, J. T., Brigham-Grette, J., Clarke, G. K. C., Cuffey, K. M., Fitzpatrick, J. J., et al. (2010). History of the Greenland Ice Sheet: paleoclimatic insights. *Quaternary Science Reviews*, *29*(15-16), 1728–1756. https://doi.org/10.1016/j.quascirev.2010.02.007

Andrews, J., Dunhill, G., Vogt, C., & Voelker, A. (2017). Denmark Strait during the Late Glacial Maximum and Marine Isotope Stage 3: Sediment sources and transport processes. *Marine Geology*, *390*, 181–198.

Andrews, J., Kirby, M., Aksu, A., Barber, D., & Meese, D. (1998). Late Quaternary detrital carbonate (DC-) layers in Baffin Bay marine sediments (67°–74° N): correlation with Heinrich events in the North Atlantic? *Quaternary Science Reviews*, *17*(12), 1125–1137.

Andrews, J. T. (2000). Icebergs and iceberg rafted detritus (IRD) in the North Atlantic: facts and assumptions. *Oceanography*, *13*, 100–108.

Austin, W. E., Wilson, L. J., & Hunt, J. B. (2004). The age and chronostratigraphical significance of North Atlantic Ash Zone II. *Journal of Quaternary Science*, *19*(2), 137–146.

Bagniewski, W., Meissner, K. J., & Menviel, L. (2017). Exploring the oxygen isotope fingerprint of Dansgaard-Oeschger variability and Heinrich events. *Quaternary Science Reviews*, *159*, 1–14.

Bard, E., Arnold, M., Mangerud, J., Paterne, M., Labeyrie, L., Duprat, J., et al. (1994). The North Atlantic atmosphere-sea surface 14C gradient during the Younger Dryas climatic event. *Earth and Planetary Science Letters*, *126*(4), 275–287. https://doi.org/10.1016/0012-821X(94)90112-0

Barker, S., Chen, J., Gong, X., Jonkers, L., Knorr, G., & Thornalley, D. (2015). Icebergs not the trigger for North Atlantic cold events. *Nature*, *520*(7547), 333–336. https://doi.org/10.1038/nature14330

Belt, S. T., Massé, G., Rowland, S. J., Poulin, M., Michel, C., & LeBlanc, B. (2007). A novel chemical fossil of palaeo sea ice: IP25. *Organic Geochemistry*, *38*(1), 16–27.

Böhm, E., Lippold, J., Gutjahr, M., Frank, M., Blaser, P., Antz, B., et al. (2015). Strong and deep Atlantic meridional overturning circulation during the last glacial cycle. *Nature*, *517*(7532), 73–76. https://doi.org/10.1038/nature14059

Bond, G. (1997). A pervasive millennial-scale cycle in North Atlantic Holocene and glacial climates. *Science*, *278*(5341), 1257–1266. https://doi.org/10.1126/science.278.5341.1257

Bond, G., Broecker, W., Johnsen, S., McManus, J., Labeyrie, L., Jouzel, J., & Bonani, G. (1993). Correlations between climate records from North Atlantic sediments and Greenland ice. *Nature*, *365*(6442), 143–147.

Bond, G., Heinrich, H., Broecker, W., Labeyrie, L., McManus, J., Andrews, J., et al. (1992). Evidence for massive discharges of icebergs into the North Atlantic ocean during the last glacial period. *Nature*, *360*(6401), 245–249. https://doi.org/10.1038/360245a0

Born, A., & Mignot, J. (2012). Dynamics of decadal variability in the Atlantic subpolar gyre: a stochastically forced oscillator. *Climate Dynamics*, *39*(1), 461–474.

Born, A., Nisancioglu, K. H., & Risebrobakken, B. (2011). Late Eemian warming in the Nordic Seas as seen in proxy data and climate models. *Paleoceanography*, *26*, PA2207. https://doi.org/10.1029/2010PA002027

Carstens, J., Hebbeln, D., & Wefer, G. (1997). Distribution of planktic foraminifera at the ice margin in the Arctic (Fram Strait). *Marine Micropaleontology*, *29*(3-4), 257–269.

Channell, J. E. T., Hodell, D. A., Romero, O., Hillaire-Marcel, C., de Vernal, A., Stoner, J. S., et al. (2012). A 750-kyr detrital-layer stratigraphy for the North Atlantic (IODP Sites U1302–U1303, Orphan Knoll, Labrador Sea). *Earth and Planetary Science Letters*, *317-318*, 218–230. https://doi.org/10.1016/j.epsl.2011.11.029

Clark, P. U., & Mix, A. C. (2002). Ice sheets and sea level of the Last Glacial Maximum. *Quaternary Science Reviews*, *21*(1-3), 1–7.

Cortijo, E., Labeyrie, L., Vidal, L., Vautravers, M., Chapman, M., Duplessy, J.-C., et al. (1997). Changes in sea surface hydrology associated with Heinrich event 4 in the North Atlantic Ocean between 40 and 60 N. *Earth and Planetary Science Letters*, *146*(1-2), 29–45. https://doi.org/10.1016/S0012-821X(96)00217-8

Cortijo, E., Yiou, P., Labeyrie, L., & Cremer, M. (1995). Sedimentary record of rapid climatic variability in the North Atlantic Ocean during the last glacial cycle. *Paleoceanography*, *10*(5), 911–926.

Daniault, N., Mercier, H., Lherminier, P., Sarafanov, A., Falina, A., Zunino, P., et al. (2016). The northern North Atlantic Ocean mean circulation in the early 21st century. *Progress in Oceanography*, *146*, 142–158. https://doi.org/10.1016/j.pocean.2016.06.007

Dansgaard, W., Johnsen, S. J., Clausen, H. B., Dahl-Jensen, D., Gundestrup, N. S., Hammer, C. U., et al. (1993). Evidence for general instability of past climate from a 250-kyr ice-core record. *Nature*, *364*(6434), 218–220. https://doi.org/10.1038/364218a0

De Schepper, S., Ray, J. L., Skaar, K. S., Sadatzki, H., Ijaz, U. Z., Stein, R., & Larsen, A. (2019). The potential of sedimentary ancient DNA for reconstructing past sea ice evolution. *The ISME Journal*, *13*(10), 2566–2577. https://doi.org/10.1038/s41396-019-0457-1

de Vernal, A., & Hillaire-Marcel, C. (2000). Sea-ice cover, sea-surface salinity and halo-/thermocline structure of the northwest North Atlantic: modern versus full glacial conditions. *Quaternary Science Reviews*, *19*(1-5), 65–85.

Death, R., Siegert, M. J., Bigg, G. R., & Wadley, M. R. (2006). Modelling iceberg trajectories, sedimentation rates and meltwater input to the ocean from the Eurasian Ice Sheet at the Last Glacial Maximum. *Palaeogeography, Palaeoclimatology, Palaeoecology*, *236*(1-2), 135–150. https://doi.org/10.1016/j.palaeo.2005.11.040

Dickson, B., Yashayaev, I., Meincke, J., Turrell, B., Dye, S., & Holfort, J. (2002). Rapid freshening of the deep North Atlantic Ocean over the past four decades. *Nature*, *416*(6883), 832–837. https://doi.org/10.1038/416832a

Dokken, T. M., Nisancioglu, K. H., Li, C., Battisti, D. S., & Kissel, C. (2013). Dansgaard-Oeschger cycles: Interactions between ocean and sea ice intrinsic to the Nordic seas. *Paleoceanography*, *28*, 491–502. https://doi.org/10.1002/palo.20042

Dowdeswell, J., Elverhøi, A., & Spielhagen, R. (1998). Glacimarine sedimentary processes and facies on the Polar North Atlantic margins. *Quaternary Science Reviews*, *17*(1-3), 243–272.

Drijfhout, S., Gleeson, E., Dijkstra, H., & Livina, V. (2013). Spontaneous abrupt climate change due to an atmospheric blocking–sea-ice–ocean feedback in an unforced climate model simulation. *Proceedings of the National Academy of Sciences of the United States of America*, *110*(49), 19,713–19,718. https://doi.org/10.1073/pnas.1304912110

Duprat, L. P. A. M., Bigg, G. R., & Wilton, D. J. (2016). Enhanced Southern Ocean marine productivity due to fertilization by giant icebergs. *Nature Geoscience*, *9*(3), 219–221. https://doi.org/10.1038/ngeo2633

Elliot, M. (2017). Paleoclimate data from core SU90-24, Irminger basin. https://doi.org/10.1594/PANGAEA.881875

Elliot, M., Labeyrie, L., Bond, G., Cortijo, E., Turon, J. L., Tisnerat, N., & Duplessy, J. C. (1998). Millennial-scale iceberg discharges in the Irminger Basin during the last glacial period: Relationship with the Heinrich events and environmental settings. *Paleoceanography*, *13*(5), 433–446.

Elliot, M., Labeyrie, L., Dokken, T., & Manthé, S. (2001). Coherent patterns of ice-rafted debris deposits in the Nordic regions during the last glacial (10–60 ka). *Earth and Planetary Science Letters*, *194*(1-2), 151–163.

Elliot, M., Labeyrie, L., & Duplessy, J.-C. (2002). Changes in North Atlantic deep-water formation associated with the Dansgaard–Oeschger temperature oscillations (60–10ka). *Quaternary Science Reviews*, *21*(10), 1153–1165.

Evans, H. F., Channell, J. E., Stoner, J. S., Hillaire-Marcel, C., Wright, J. D., Neitzke, L. C., & Mountain, G. S. (2007). Paleointensity-assisted chronostratigraphy of detrital layers on the Eirik Drift (North Atlantic) since marine isotope stage 11. *Geochemistry, Geophysics, Geosystems*, *8*, Q11007. https://doi.org/10.1029/2007GC001720

Ezat, M. M., Rasmussen, T. L., & Groeneveld, J. (2014). Persistent intermediate water warming during cold stadials in the southeastern Nordic seas during the past 65 ky. *Geology*, *42*(8), 663–666.

Frogner, P., Gíslason, S. R., & Óskarsson, N. (2001). Fertilizing potential of volcanic ash in ocean surface water. *Geology*, *29*(6), 487–490.

Funder, S., Jennings, A., & Kelly, M. (2004). Middle and late Quaternary glacial limits in Greenland. In *Developments in Quaternary Sciences* (Vol. 2, pp. 425–430). Elsevier.

Funder, S., Kjeldsen, K. K., Kjær, K. H., & Cofaigh, C. Ó. (2011). The Greenland Ice Sheet during the past 300,000 years: A review. In *Developments in Quaternary Sciences* (Vol. 15, pp. 699–713). Elsevier.

Galaasen, E. V., Ninnemann, U. S., Irvalı, N., Kleiven, H. K. F., Rosenthal, Y., Kissel, C., & Hodell, D. A. (2014). Rapid reductions in North Atlantic Deep Water during the peak of the last interglacial period. *Science*, *343*(6175), 1129–1132. https://doi.org/10.1126/science.1248667

Ganopolski, A., Calov, R., & Claussen, M. (2010). Simulation of the last glacial cycle with a coupled climate ice-sheet model of intermediate complexity. *Climate of the Past*, *6*(2), 229–244.

Garcia-Ibanez, M. I., Pérez, F. F., Lherminier, P., Zunino, P., Mercier, H., & Tréguer, P. (2018). Water mass distributions and transports for the 2014 GEOVIDE cruise in the North Atlantic. *Biogeosciences*, *15*(7), 2075–2090.

Greco, M., Jonkers, L., Kretschmer, K., Bijma, J., & Kucera, M. (2019). Variable habitat depth of the planktonic foraminifera Neogloboquadrina pachyderma in the northern high latitudes explained by sea-ice and chlorophyll concentration. *Biogeosciences Discuss*, *2019*, 1–30. https://doi.org/10.5194/bg-2019-79

Grousset, F. E., Cortijo, E., Huon, S., Hervé, L., Richter, T., Burdloff, D., et al. (2001). Zooming in on Heinrich layers. *Paleoceanography*, *16*(3), 240–259. https://doi.org/10.1029/2000PA000559

Grousset, F. E., Labeyrie, L., Sinko, J. A., Cremer, M., Bond, G., Duprat, J., et al. (1993). Patterns of ice-rafted detritus in the glacial North Atlantic (40–55° N). *Paleoceanography*, *8*(2), 175–192. https://doi.org/10.1029/92PA02923

Hagen, S., & Hald, M. (2002). Variation in surface and deep water circulation in the Denmark Strait, North Atlantic, during marine isotope stages 3 and 2. *Paleoceanography and Paleoclimatology*, *17*(4), 1061. https://doi.org/10.1029/2001PA000632

Hátún, H., Sandø, A. B., Drange, H., Hansen, B., & Valdimarsson, H. (2005). Influence of the Atlantic subpolar gyre on the thermohaline circulation. *Science*, *309*(5742), 1841–1844. https://doi.org/10.1126/science.1114777

Heinrich, H. (1988). Origin and consequences of cyclic ice rafting in the northeast Atlantic Ocean during the past 130,000 years. *Quaternary Research*, *29*(2), 142–152.

Hemming, S. R. (2004). Heinrich events: Massive late Pleistocene detritus layers of the North Atlantic and their global climate imprint. *Reviews of Geophysics*, *42*, RG1005. https://doi.org/10.1029/2003RG000128

Henry, L., McManus, J. F., Curry, W. B., Roberts, N. L., Piotrowski, A. M., & Keigwin, L. (2016). North Atlantic ocean circulation and abrupt climate change during the last glaciation. *Science*, *353*(6298), 470–474. https://doi.org/10.1126/science.aaf5529

Hesse, R., & Khodabakhsh, S. (2017). Reprint of Anatomy of Labrador Sea Heinrich layers. *Marine Geology*, *393*, 67–92.

Hesse, R., Rashid, H., & Khodabakhsh, S. (2004). Fine-grained sediment lofting from meltwater-generated turbidity currents during Heinrich events. *Geology*, *32*(5), 449–452.

Hillaire-Marcel, C., de Vernal, A., & McKay, J. (2011). Foraminifer isotope study of the Pleistocene Labrador Sea, northwest North Atlantic (IODP Sites 1302/03 and 1305), with emphasis on paleoceanographical differences between its "inner" and "outer" basins. *Marine Geology*, *279*(1), 188–198.

Hillaire-Marcel, C., Vernal, A. d., Bilodeau, G., & Wu, G. (1994). Isotope stratigraphy, sedimentation rates, deep circulation, and carbonate events in the Labrador Sea during the last~ 200 ka. *Canadian Journal of Earth Sciences*, *31*(1), 63–89.

Hiscott, R. N., Aksu, A. E., Mudie, P. J., & Parsons, D. F. (2001). A 340,000 year record of ice rafting, palaeoclimatic fluctuations, and shelf-crossing glacial advances in the southwestern Labrador Sea. *Global and Planetary Change*, *28*(1-4), 227–240.

Hoff, U., Rasmussen, T. L., Stein, R., Ezat, M. M., & Fahl, K. (2016). Sea ice and millennial-scale climate variability in the Nordic seas 90[thinsp]kyr ago to present. *Nat Commun*, *7*(1), 1–10. https://doi.org/10.1038/ncomms12247

Holliday, N. P., Meyer, A., Bacon, S., Alderson, S. G., & de Cuevas, B. (2007). Retroflection of part of the east Greenland current at Cape Farewell. *Geophysical Research Letters*, *34*, L07609. https://doi.org/10.1029/2006GL029085

Hopkins, T. S. (1991). The GIN Sea—A synthesis of its physical oceanography and literature review 1972–1985. *Earth-Science Reviews*, *30*(3-4), 175–318.

Huber, C., Leuenberger, M., Spahni, R., Flückiger, J., Schwander, J., Stocker, T. F., et al. (2006). Isotope calibrated Greenland temperature record over Marine Isotope Stage 3 and its relation to CH4. *Earth and Planetary Science Letters*, *243*(3-4), 504–519.

Huck, T. (2010). Recent changes in the North Atlantic circulation. Paper presented at the Iceland in the Central Northern Atlantic: hotspot, sea currents and climate change.

Hunter, S., Wilkinson, D., Louarn, E., McCave, I. N., Rohling, E., Stow, D. A., & Bacon, S. (2007). Deep western boundary current dynamics and associated sedimentation on the Eirik Drift, Southern Greenland Margin. *Deep Sea Research Part I: Oceanographic Research Papers*, *54*(12), 2036–2066.

Hunter, S., Wilkinson, D., Stanford, J., Stow, D., Bacon, S., Akhmetzhanov, A., & Kenyon, N. (2007). The Eirik Drift: a long-term barometer of North Atlantic deepwater flux south of Cape Farewell, Greenland. *Geological Society, London, Special Publications*, *276*(1), 245–263.

ice2ice (2016). Ice2Ice Cruise GS16-204, 16. Aug - 5. Sept 2016. Retrieved from https://www.bcdc.no/files/bcdc-theme/documents/GS16-204_cruise%20report.pdf

Irvalı, N., Ninnemann, U. S., Kleiven, H. K. F., Galaasen, E. V., Morley, A., & Rosenthal, Y. (2016). Evidence for regional cooling, frontal advances, and East Greenland Ice Sheet changes during the demise of the last interglacial. *Quaternary Science Reviews*, *150*, 184–199.

Jansen, E. (1989). The use of stable oxygen and carbon isotope stratigraphy as a dating tool. *Quaternary international*, *1*, 151–166.

Johannessen, T., Jansen, E., Flatøy, A., & Ravelo, A. C. (1994). The relationship between surface water masses, oceanographic fronts and paleoclimatic proxies in surface sediments of the Greenland, Iceland, Norwegian Seas. In *Carbon cycling in the glacial ocean: constraints on the ocean's role in global change* (pp. 61–85). Springer.

Kleppin, H., Jochum, M., Otto-Bliesner, B., Shields, C. A., & Yeager, S. (2015). Stochastic Atmospheric Forcing as a Cause of Greenland Climate Transitions. *Journal of Climate*, *28*(19).

Knutz, P. C., Sicre, M. A., Ebbesen, H., Christiansen, S., & Kuijpers, A. (2011). Multiple-stage deglacial retreat of the southern Greenland Ice Sheet linked with Irminger Current warm water transport. *Paleoceanography*, *26*, PA3204. https://doi.org/10.1029/2010PA002053

Kohfeld, K. E., Fairbanks, R. G., Smith, S. L., & Walsh, I. D. (1996). Neogloboquadrina pachyderma (sinistral coiling) as paleoceanographic tracers in polar oceans: Evidence from Northeast Water Polynya plankton tows, sediment traps, and surface sediments. *Paleoceanography*, *11*(6), 679–699.

Kozdon, R., Eisenhauer, A., Weinelt, M., Meland, M. Y., & Nürnberg, D. (2009). Reassessing Mg/Ca temperature calibrations of Neogloboquadrina pachyderma (sinistral) using paired δ44/40Ca and Mg/Ca measurements. *Geochemistry, Geophysics, Geosystems*, *10*, Q03005. https://doi.org/10.1029/2008GC002169

Labeyrie, L., Leclaire, H., Waelbroeck, C., Cortijo, E., Jean-Claude, D., Vidal, L., et al. (1999). Temporal variability of the surface and deep waters of the North West Atlantic Ocean at orbital and millennial scales. *Geophysical Monograph-American Geophysical Union*, *112*, 77–98.

Lackschewitz, K. S., Baumann, K.-H., Gehrke, B., Wallrabe-Adams, H.-J., Thiede, J., Bonani, G., et al. (1998). North Atlantic ice sheet fluctuations 10,000–70,000 yr ago as inferred from deposits on the Reykjanes Ridge, southeast of Greenland. *Quaternary research*, *49*(2), 171–182. https://doi.org/10.1006/qres.1997.1948

Lambeck, K., Yokoyama, Y., & Purcell, T. (2002). Into and out of the Last Glacial Maximum: sea-level change during Oxygen Isotope Stages 3 and 2. *Quaternary Science Reviews*, *21*(1-3), 343–360.

Laskar, J., Robutel, P., Joutel, F., Gastineau, M., Correia, A., & Levrard, B. (2004). A long-term numerical solution for the insolation quantities of the Earth. *Astronomy & Astrophysics*, *428*(1), 261–285.

Li, C., Battisti, D. S., & Bitz, C. M. (2010). Can North Atlantic sea ice anomalies account for Dansgaard–Oeschger climate signals? *Journal of Climate*, *23*(20), 5457–5475.

Li, C., & Born, A. (2019). Coupled atmosphere-ice-ocean dynamics in Dansgaard-Oeschger events. *Quaternary Science Reviews*, *203*, 1–20.

McCave, I., & Tucholke, B. (1986). Deep current-controlled sedimentation in the western North Atlantic. *The Geology of North America*, *1000*, 451–468.

Mignot, J., Ganopolski, A., & Levermann, A. (2007). Atlantic subsurface temperatures: Response to a shutdown of the overturning circulation and consequences for its recovery. *Journal of Climate*, *20*(19), 4884–4898.

Moffa-Sánchez, P., Hall, I. R., Barker, S., Thornalley, D. J., & Yashayaev, I. (2014). Surface changes in the eastern Labrador Sea around the onset of the Little Ice Age. *Paleoceanography*, *29*, 160–175. https://doi.org/10.1002/2013PA002523

Müller-Michaelis, A., & Uenzelmann-Neben, G. (2014). Development of the Western Boundary Undercurrent at Eirik Drift related to changing climate since the early Miocene. *Deep Sea Research Part I: Oceanographic Research Papers*, *93*, 21–34.

Naafs, B. D. A., Hefter, J., Gruetzner, J., & Stein, R. (2013). Warming of surface waters in the mid-latitude North Atlantic during Heinrich events. *Paleoceanography*, *28*, 153–163. https://doi.org/10.1029/2012PA002354

Nicholl, J. A., Hodell, D. A., Naafs, B. D. A., Hillaire-Marcel, C., Channell, J. E., & Romero, O. E. (2012). A Laurentide outburst flooding event during the last interglacial period. *Nature Geoscience*, *5*(12), 901.

Paillard, D., Labeyrie, L., & Yiou, P. (1996). Macintosh program performs time-series analysis. *Eos, Transactions American Geophysical Union*, *77*(39), 379–379.

Patton, H., Hubbard, A., Andreassen, K., Winsborrow, M., & Stroeven, A. P. (2016). The build-up, configuration, and dynamical sensitivity of the Eurasian ice-sheet complex to Late Weichselian climatic and oceanic forcing. *Quaternary Science Reviews*, *153*, 97–121.

Peck, V. L., Hall, I. R., Zahn, R., Grousset, F., Hemming, S., & Scourse, J. (2007). The relationship of Heinrich events and their European precursors over the past 60ka BP: a multi-proxy ice-rafted debris provenance study in the North East Atlantic. *Quaternary Science Reviews*, *26*(7), 862–875.

Pflaumann, U., Duprat, J., Pujol, C., & Labeyrie, L. D. (1996). SIMMAX: A modern analog technique to deduce Atlantic sea surface temperatures from planktonic foraminifera in deep-sea sediments. *Paleoceanography*, *11*(1), 15–35.

Pflaumann, U., Sarnthein, M., Chapman, M., d'Abreu, L., Funnell, B., Huels, M., et al. (2003). Glacial North Atlantic: Sea-surface conditions reconstructed by GLAMAP 2000. *Paleoceanography*, *18*(3), 1065. https://doi.org/10.1029/2002PA000774

Rahman, A., & de Vernal, A. (1994). Surface oceanographic changes in the eastern Labrador Sea: Nannofossil record of the last 31,000 years. *Marine Geology*, *121*(3-4), 247–263.

Rahmstorf, S. (2002). Ocean circulation and climate during the past 120,000 years. *Nature*, *419*(6903), 207–214. https://doi.org/10.1038/nature01090

Ramseier, R. O., Garrity, C., & Martin, T. (2001). An overview of sea-ice conditions in the Greenland Sea and the relationship of oceanic sedimentation to the ice regime. In *The Northern North Atlantic* (pp. 19–38). Springer.

Rashid, H., Hesse, R., & Piper, D. J. (2003a). Distribution, thickness and origin of Heinrich layer 3 in the Labrador Sea. *Earth and Planetary Science Letters*, *205*(3-4), 281–293.

Rashid, H., Hesse, R., & Piper, D. J. (2003b). Evidence for an additional Heinrich event between H5 and H6 in the Labrador Sea. *Paleoceanography*, *18*(4), 1077. https://doi.org/10.1029/2003PA000913

Rasmussen, T. L., & Thomsen, E. (2004). The role of the North Atlantic Drift in the millennial timescale glacial climate fluctuations. *Palaeogeography, Palaeoclimatology, Palaeoecology*, *210*(1), 101–116.

Reimer, P. J., Bard, E., Bayliss, A., Beck, J. W., Blackwell, P. G., Ramsey, C. B., et al. (2013). IntCal13 and Marine13 radiocarbon age calibration curves 0–50,000 years cal BP. *Radiocarbon*, *55*(4), 1869–1887. https://doi.org/10.2458/azu_js_rc.55.16947

Rhein, M., Kieke, D., Hüttl-Kabus, S., Roessler, A., Mertens, C., Meissner, R., et al. (2011). Deep water formation, the subpolar gyre, and the meridional overturning circulation in the subpolar North Atlantic. *Deep Sea Research Part II: Topical Studies in Oceanography*, *58*(17-18), 1819–1832. https://doi.org/10.1016/j.dsr2.2010.10.061

Ruddiman, W. F. (1977). Late Quaternary deposition of ice-rafted sand in the subpolar North Atlantic (lat 40 to 65 N). *Geological Society of America Bulletin*, *88*(12), 1813–1827.

Sadatzki, H., Dokken, T. M., Berben, S. M. P., Muschitiello, F., Stein, R., Fahl, K., et al. (2019). Sea ice variability in the southern Norwegian Sea during glacial Dansgaard-Oeschger climate cycles. *Science Advances*, *5*(3). https://doi.org/10.1126/sciadv.aau6174

Sarnthein, M., Balmer, S., Grootes, P. M., & Mudelsee, M. (2015). Planktic and benthic 14 C reservoir ages for three ocean basins, calibrated by a suite of 14 C plateaus in the glacial-to-deglacial Suigetsu atmospheric 14 C record. *Radiocarbon*, *57*(1), 129–151.

Sarnthein, M., Stattegger, K., Dreger, D., Erlenkeuser, H., Grootes, P., Haupt, B., et al. (2001). Fundamental Modes and Abrupt Changes in North Atlantic Circulation and Climate over the last 60 ky–Concepts, Reconstruction and Numerical Modeling. The Northern North Atlantic: A changing environment., 365-410.

Schlitzer, R. (2015). Ocean Data View. Retrieved from odv.awi.de

Schwarz, J., & Schodlok, M. (2009). Impact of drifting icebergs on surface phytoplankton biomass in the Southern Ocean: Ocean colour remote sensing and in situ iceberg tracking. *Deep Sea Research Part I: Oceanographic Research Papers*, *56*(10), 1727–1741.

Seierstad, I. K., Abbott, P. M., Bigler, M., Blunier, T., Bourne, A. J., Brook, E., et al. (2014). Consistently dated records from the Greenland GRIP, GISP2 and NGRIP ice cores for the past 104 ka reveal regional millennial-scale δ18O gradients with possible Heinrich event imprint. *Quaternary Science Reviews*, *106*, 29–46.

Sessford, E., Tisserand, A., Risebrobakken, B., Andersson, C., Dokken, T., & Jansen, E. (2018). High-Resolution Benthic Mg/Ca Temperature Record of the Intermediate Water in the Denmark Strait Across D-O Stadial-Interstadial Cycles. *Paleoceanography and Paleoclimatology*, *33*, 1169–1185. https://doi.org/10.1029/2018PA003370

Simstich, J., Sarnthein, M., & Erlenkeuser, H. (2003). Paired δ 18 O signals of Neogloboquadrina pachyderma (s) and Turborotalita quinqueloba show thermal stratification structure in Nordic Seas. *Marine Micropaleontology*, *48*(1), 107–125.

Smith, K. L., Robison, B. H., Helly, J. J., Kaufmann, R. S., Ruhl, H. A., Shaw, T. J., et al. (2007). Free-drifting icebergs: hot spots of chemical and biological enrichment in the Weddell Sea. *Science*, *317*(5837), 478–482. https://doi.org/10.1126/science.1142834

Stein, R., Nam, S.-I., Grobe, H., & Hubberten, H. (1996). Late Quaternary glacial history and short-term ice-rafted debris fluctuations along the East Greenland continental margin. *Geological Society, London, Special Publications*, *111*(1), 135–151.

Stern, A. A., Johnson, E., Holland, D. M., Wagner, T. J. W., Wadhams, P., Bates, R., et al. (2015). Wind-driven upwelling around grounded tabular icebergs. *Journal of Geophysical Research: Oceans*, *120*, 5820–5835. https://doi.org/10.1002/2015JC010805

Stoner, J., Channell, J., & Hillaire-Marcel, C. (1998). A 200 ka geomagnetic chronostratigraphy for the Labrador Sea: Indirect correlation of the sediment record to SPECMAP. *Earth and Planetary Science Letters*, *159*(3), 165–181.

Stoner, J. S., Channell, J. E., & Hillaire-Marcel, C. (1996). The magnetic signature of rapidly deposited detrital layers from the Deep Labrador Sea: Relationship to North Atlantic Heinrich layers. *Paleoceanography*, *11*, 309–325.

Straneo, F., & Heimbach, P. (2013). North Atlantic warming and the retreat of Greenland's outlet glaciers. *Nature*, *504*(7478), 36–43. https://doi.org/10.1038/nature12854

Straneo, F., Sutherland, D. A., Holland, D., Gladish, C., Hamilton, G. S., Johnson, H. L., et al. (2012). Characteristics of ocean waters reaching Greenland's glaciers. *Annals of Glaciology*, *53*, 60.

Svendsen, J. I., Alexanderson, H., Astakhov, V. I., Demidov, I., Dowdeswell, J. A., Funder, S., et al. (2004). Late Quaternary ice sheet history of northern Eurasia. *Quaternary Science Reviews*, *23*(11-13), 1229–1271. https://doi.org/10.1016/j.quascirev.2003.12.008

Svensson, A., Andersen, K. K., Bigler, M., Clausen, H. B., Dahl-Jensen, D., Davies, S. M., et al. (2008). A 60 000 year Greenland stratigraphic ice core chronology. *Climate of the Past*, *4*(1), 47–57. https://doi.org/10.5194/cp-4-47-2008

Thornalley, D. J. R., Oppo, D. W., Ortega, P., Robson, J. I., Brierley, C. M., Davis, R., et al. (2018). Anomalously weak Labrador Sea convection and Atlantic overturning during the past 150 years. *Nature*, *556*(7700), 227–230. https://doi.org/10.1038/s41586-018-0007-4

van Kreveld, S., Sarnthein, M., Erlenkeuser, H., Grootes, P., Jung, S., Nadeau, M. J., et al. (2000). Potential links between surging ice sheets, circulation changes, and the Dansgaard-Oeschger cycles in the Irminger Sea, 60–18 kyr. *Paleoceanography*, *15*(4), 425–442. https://doi.org/10.1029/1999PA000464

Vasskog, K., Langebroek, P. M., Andrews, J. T., Nilsen, J. E. Ø., & Nesje, A. (2015). The Greenland Ice Sheet during the last glacial cycle: Current ice loss and contribution to sea-level rise from a palaeoclimatic perspective. *Earth-Science Reviews*, *150*, 45–67.

Vettoretti, G., & Peltier, W. R. (2016). Thermohaline instability and the formation of glacial North Atlantic super polynyas at the onset of Dansgaard-Oeschger warming events. *Geophysical Research Letters*, *43*, 5336–5344. https://doi.org/10.1002/2016GL068891

Vidal, L., Labeyrie, L., Cortijo, E., Arnold, M., Duplessy, J. C., Michel, E., et al. (1997). Evidence for changes in the North Atlantic Deep Water linked to meltwater surges during the Heinrich events. *Earth and Planetary Science Letters*, *146*(1-2), 13–27. https://doi.org/10.1016/S0012-821X(96)00192-6

Voelker, A. H., Grootes, P. M., Nadeau, M.-J., & Sarnthein, M. (2000). Radiocarbon levels in the Iceland Sea from 25–53 kyr and their link to the Earth's magnetic field intensity. *Radiocarbon*, *42*(3), 437–452.

Voelker, A. H., & Haflidason, H. (2015a). Refining the Icelandic tephrachronology of the last glacial period–the deep-sea core PS2644 record from the southern Greenland Sea. *Global and Planetary Change*, *131*, 35–62.

Voelker, A. H., Sarnthein, M., Grootes, P. M., & Schleicher, M. (1998). Correlation of marine 14C ages from the Nordic Seas with the GISP2 isotope record: Implications for 14C calibration beyond 25 ka BP. Paper presented at the Radiocarbon.

Voelker, A. H. L. (2018). Calendar Age based age model for core SU90-24. https://doi.org/10.1594/PANGAEA.886728

Voelker, A. H. L., & Haflidason, H. (2015b). Deep-sea sediment core PS2644 record from the southern Greenland Sea. *Global and Planetary Change* Retrieved from, *131*, 35–62. https://doi.org/10.1594/PANGAEA.831474

Waelbroeck, C., Duplessy, J.-C., Michel, E., Labeyrie, L., Paillard, D., & Duprat, J. (2001). The timing of the last deglaciation in North Atlantic climate records. *Nature*, *412*(6848), 724–727. https://doi.org/10.1038/35089060

Waelbroeck, C., Labeyrie, L., Michel, E., Duplessy, J. C., McManus, J. F., Lambeck, K., et al. (2002). Sea-level and deep water temperature changes derived from benthic foraminifera isotopic records. *Quaternary Science Reviews*, *21*(1-3), 295–305. https://doi.org/10.1016/S0277-3791(01)00101-9

White, L. F., Bailey, I., Foster, G. L., Allen, G., Kelley, S. P., Andrews, J. T., et al. (2016). Tracking the provenance of Greenland-sourced, Holocene aged, individual sand-sized ice-rafted debris using the Pb-isotope compositions of feldspars and 40Ar/39Ar ages of hornblendes. *Earth and Planetary Science Letters*, *433*, 192–203. https://doi.org/10.1016/j.epsl.2015.10.054

Yashayaev, I., Seidov, D., & Demirov, E. (2015). *A new collective view of oceanography of the Arctic and North Atlantic basins*. Elsevier.